

The Modular Flow in Three Homeomorphic Spaces

A Thesis
Presented to
The Division of Mathematics and Natural Sciences
Reed College

In Partial Fulfillment
of the Requirements for the Degree
Bachelor of Arts

Christopher Henn

May 2018

Approved for the Division
(Mathematics)

Kyle M. Ormsby

Acknowledgements

Many thanks,

- to Kyle, for his unceasing help in creating this thesis;
- to my friends at O-Town, a cheery bunch, and to those at Reed;
- and to my parents, for conceiving my existence and providing unconditional love and support.

I am deeply indebted to you all. Thank you!

Table of Contents

Introduction	1
Chapter 1: The Space of Lattices	3
1.1 The Modular Flow of Lattices	4
1.2 The Classical Perspective on the Modular Flow	7
Chapter 2: The 3-sphere and the Trefoil Complement	11
2.1 The Fundamental Group of the Trefoil Complement	11
2.2 From \mathcal{L} to S^3	16
2.3 The Linking Number of Periodic Orbits in S^3	17
Chapter 3: Finite Subsets of the Circle	27
3.1 Topologizing $\exp_k X$	27
3.2 From \mathcal{L} to $\exp_3 S^1$	29
3.3 Visualizing the Generators of B_3 in $\exp_{\{2,3\}} S^1$	30
3.4 Diagrammatic Decompositions of Hyperbolic Subset Loops	33
3.5 The Linking Number of Finite Subset Loops	35
Appendix A: Computational Exploration of Homeomorphisms	39
A.1 Visualizing a Dynamical System in the Space of Lattices	40
A.2 Coding the Homeomorphism from $\mathcal{L} \rightarrow S^3$	41
A.3 Coding the Homeomorphism from $\mathcal{L} \rightarrow \exp_3 S^1$	44
Appendix B: Supplemental Data	47
Bibliography	51

Abstract

In this thesis we describe the modular flow, a dynamical system in a space of lattices \mathcal{L}_1 . The modular flow is closely connected to a classically studied dynamical system—the geodesic flow on the modular surface—and presents in numerous and diverse fields of study. We detail a recent knot-theoretic finding concerning the periodic orbits of the modular flow from the work of E. Ghys in 2007. We then analyze periodic orbits of the modular flow in $\exp_{\{2,3\}} S^1 \cong \mathcal{L}_1$, a seldom-studied space consisting of all two- and three-point subsets of the circle S^1 . Using our analysis of the modular flow in $\exp_{\{2,3\}} S^1$, we present a computer-aided diagrammatic system for decomposing homotopy-classes of periodic orbits as braids in the braid group B_3 . We finish with a conjecture relating these diagrams to the results of Ghys.

Introduction

The 3-sphere, the space of nontrivial lattices, and 1 to 3 point subsets of the circle—each of these spaces possesses a unique and rich structure. Remarkably, they are also homeomorphic, providing multiple perspectives of phenomena occurring in each space individually.

In this document, we examine the modular flow and its periodic orbits in the space of nontrivial lattices. This is a dynamical system whose periodic orbits can be described in terms of hyperbolic elements of the modular group, $\mathrm{PSL}_2\mathbb{Z}$. Viewed in the 3-sphere, such a flow presents as a link with the trefoil knot. A basic property of these trefoil links, their linking number, can be described by a classic yet mysterious arithmetic function. Moreover, the knot-complement of the trefoil in the 3-sphere has fundamental group isomorphic to a famous group, the braid group on 3 strands, providing an additional viewpoint from which to consider periodic orbits of lattices and their associated trefoil links.

The space of finite subsets of the circle is perhaps the most obscure of the aforementioned spaces, having been studied little in comparison to the space of lattices and the 3-sphere. The modular flow in this finite subset space begs a visual interpretation similar to that of the trefoil links in the 3-sphere. Here, we examine the group theoretic interpretation of finite subset loops as elements of the braid group. Additionally, we provide a conjecture for determining the linking number of a trefoil link from such a loop.

This document will proceed by examining each homeomorphic space in turn.

Chapter 1

The Space of Lattices

First, we recall some necessary definitions. A **lattice in \mathbb{R}^2** is a discrete, closed, and additive subgroup of \mathbb{R}^2 . If a lattice L is isomorphic to \mathbb{Z} or $\mathbb{Z} \oplus \mathbb{Z}$, then we say that L is a **degenerate** or **nondegenerate** lattice, respectively. If L is isomorphic to the trivial group, then L is the **zero lattice**. A lattice of each type is shown in Figure 1.1.

We can construct any nondegenerate lattice using a real 2×2 matrix whose columns are linearly independent. If B is such a matrix, then

$$B(\mathbb{Z}^2) = \{Bx : x \in \mathbb{Z}^2\}$$

is the **lattice generated by B** . We call B a **basis** for the lattice and the columns of B the **generators** of the lattice. Degenerate lattices can be similarly constructed using a single generator.

Two lattices L and L' are **homothetic** if they are rescaled versions of each other, i.e. if $L' = tL = \{tx : x \in L\}$ for some fixed nonzero $t \in \mathbb{R}$. We denote the space of all nontrivial lattices modulo the homothety relation as

$$\mathcal{L} = \mathcal{L}_0 \cup \mathcal{L}_1$$

where \mathcal{L}_0 and \mathcal{L}_1 are the degenerate and nondegenerate lattices, respectively.

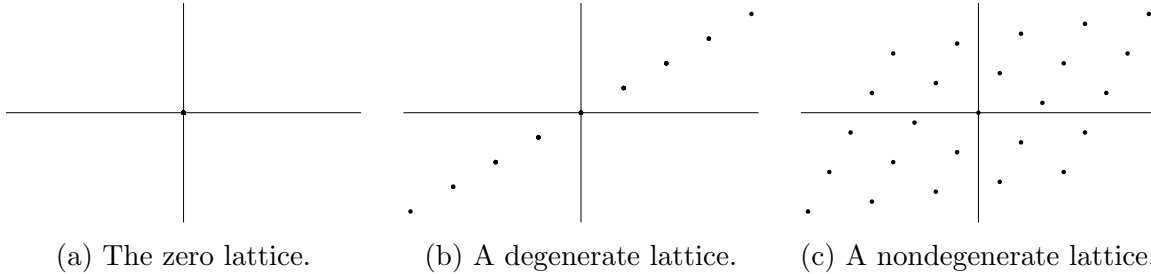


Figure 1.1: The three types of lattices.

1.1 The Modular Flow of Lattices

We now describe a dynamical flow in the space of nondegenerate lattices. Left multiplication of each point in a nondegenerate lattice by

$$\delta_t = \begin{pmatrix} \exp(t) & 0 \\ 0 & \exp(-t) \end{pmatrix} \quad (1.1)$$

produces another nondegenerate lattice (where $t \in \mathbb{R}^+$). As the time variable t increases continuously, we obtain a flow in \mathcal{L}_1 known as **the modular flow** [Ghy07; LG; BW14].

Note that as t increases, each individual point in the lattice moves towards $\pm\infty$ along a hyperbolic path, yet the lattice as a whole may move back to its original position. Thus we can study the periodic orbits of this flow.

These periodic orbits can be described succinctly via a particular type of matrix. Recall that the **special linear group** $\mathrm{SL}_2\mathbb{Z}$ is the set of 2×2 matrices with integer entries and determinant 1. The **projective special linear group** $\mathrm{PSL}_2\mathbb{Z}$ is $\mathrm{SL}_2\mathbb{Z}/\{\pm I\}$. We say that a matrix

$$A = \begin{pmatrix} a & b \\ c & d \end{pmatrix} \in \mathrm{PSL}_2\mathbb{Z}$$

is **hyperbolic** if $|a + d| > 2$. Hyperbolic matrices are diagonalizable over the real numbers, so we can find a real 2×2 matrix P such that

$$PAP^{-1} = \begin{pmatrix} \lambda_1 & 0 \\ 0 & \lambda_2 \end{pmatrix}$$

where λ_1 and λ_2 are the eigenvalues of A . Since $A = -A$ in $\mathrm{PSL}_2\mathbb{Z}$, we can assume that λ_1 is positive. Then since $\det(A) = 1$ and the product of eigenvalues of a matrix is equal to its determinant, we can find P such that

$$PAP^{-1} = \begin{pmatrix} \exp(T) & 0 \\ 0 & \exp(-T) \end{pmatrix} = \delta_T$$

for some $T \in \mathbb{R}$. Then

$$\begin{aligned}\delta_T P(\mathbb{Z}^2) &= PAP^{-1}P(\mathbb{Z}^2) \\ &= PA(\mathbb{Z}^2) \\ &= P(\mathbb{Z}^2)\end{aligned}\quad (\text{see Lemma 1.2}).$$

Thus the image of $P(\mathbb{Z}^2)$ by δ_t as $0 \leq t \leq T$ is a periodic orbit of orbit time T . To summarize, we have the following proposition.

Proposition 1.1. Every hyperbolic element in $\mathrm{PSL}_2\mathbb{Z}$ defines a periodic orbit of the modular flow.

For a concrete example of these periodic orbits, consider the hyperbolic matrix

$$A = \begin{pmatrix} 2 & 1 \\ 1 & 1 \end{pmatrix} \in \mathrm{PSL}_2\mathbb{Z}$$

The eigenvalues of A yield a diagonal matrix D such that $PAP^{-1} = D$, where P is the matrix whose columns are the eigenvectors of A . Explicitly, we compute that

$$D = \begin{pmatrix} (3 + \sqrt{5})/2 & 0 \\ 0 & (3 - \sqrt{5})/2 \end{pmatrix}, \quad P = \begin{pmatrix} (1 + \sqrt{5})/2 & 1 \\ (1 - \sqrt{5})/2 & 1 \end{pmatrix}.$$

Let λ be the first eigenvalue of A . We know that $D = \delta_T$ for some T , hence $\lambda = e^T$ and $T \approx 0.96$ is the orbit time for the periodic orbit corresponding to A . If we continuously act upon P by δ_t as $0 \leq t \leq T$, we observe a periodic orbit in the space of lattices. This orbit is visualized in Figure 1.2.

It is convenient to label a periodic orbit of the modular flow by the matrix $A \in \mathrm{PSL}_2\mathbb{Z}$ that produced it. But does every periodic orbit arise from an element of $\mathrm{PSL}_2\mathbb{Z}$? The following results establish that this is indeed the case.

Lemma 1.2. Matrices X and Y in $\mathrm{PSL}_2\mathbb{R}$ generate the same lattice if and only if $X = YA$ for some $A \in \mathrm{PSL}_2\mathbb{Z}$. In particular, if X generates the square lattice, then $X \in \mathrm{PSL}_2\mathbb{Z}$.

Proof. Suppose that X and Y generate the same lattice. Since a lattice consists of all integer linear combinations of its generators, we know that there exists some integer matrix A such that $X = YA$. Because X and Y are in $\mathrm{PSL}_2\mathbb{R}$, we also know that $\det(X) = \det(Y) = 1$. Then

$$1 = \det(X) = \det(YA) = \det(Y) \det(A) = 1 \cdot \det(A)$$

and so $\det(A) = 1$ and $A \in \mathrm{PSL}_2\mathbb{Z}$.

To show the converse, suppose instead that $X = YA$ for some $A \in \mathrm{PSL}_2\mathbb{Z}$. Then

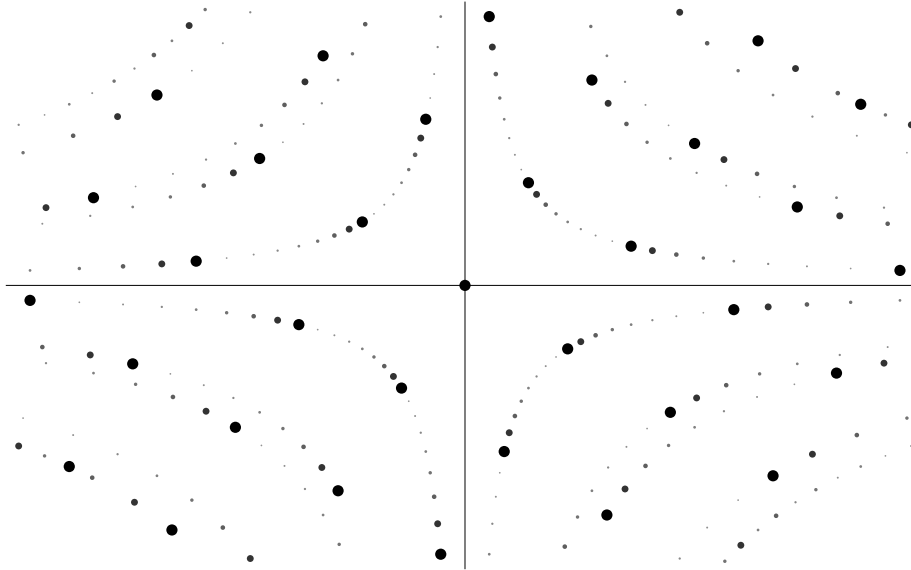


Figure 1.2: A periodic orbit of the modular flow in the space of lattices. As each point in the lattice given by P is acted upon by δ_t , it moves on a hyperbolic path towards infinity. Here, the path of each point is depicted by a sequence of points with shrinking radii. At $T \approx 0.96$, we have that $\delta_T P(\mathbb{Z}^2) = P(\mathbb{Z}^2)$.

each column of X is in $Y(\mathbb{Z}^2)$, thus $X(\mathbb{Z}^2) \subseteq Y(\mathbb{Z}^2)$. In addition, $Y = XA^{-1}$ and $A^{-1} \in \mathrm{PSL}_2\mathbb{Z}$, so similarly we have that $Y(\mathbb{Z}^2) \subseteq X(\mathbb{Z}^2)$.

If X generates the square lattice, then $X(\mathbb{Z}^2) = I(\mathbb{Z}^2)$, and so $X = IA = A \in \mathrm{PSL}_2\mathbb{Z}$. \square

Proposition 1.3. The periodic orbits of the modular flow are in bijection with conjugacy classes of elements of $\mathrm{PSL}_2\mathbb{Z}$.

Proof. Given a matrix $A \in \mathrm{PSL}_2\mathbb{Z}$, we have already shown how to construct a periodic orbit of the modular flow. It remains to be shown that any element in the conjugacy class of A produces the same periodic orbit, and that any periodic orbit of the modular flow defines the conjugacy class of some hyperbolic element in $\mathrm{PSL}_2\mathbb{Z}$. Let $P \in \mathrm{PSL}_2\mathbb{R}$ such that $PAP^{-1} = \delta_t$ for some $t \in \mathbb{R}$, so that $\delta_t P(\mathbb{Z}^2) = P(\mathbb{Z}^2)$. Also suppose that $B \in \mathrm{PSL}_2\mathbb{Z}$ as well, so that BAB^{-1} is in the conjugacy class of A . Then

$$(PB^{-1})BAB^{-1}(PB^{-1})^{-1} = PAP^{-1} = \delta_t$$

but also

$$(PB^{-1})(\mathbb{Z}^2) = P(B^{-1}(\mathbb{Z}^2)) = P(\mathbb{Z}^2).$$

Hence the element $BAB^{-1} \in \mathrm{PSL}_2\mathbb{Z}$ defines a periodic orbit with the same orbit time and same initial lattice $P(\mathbb{Z}^2)$, i.e. the same periodic orbit as A .

Now, suppose instead that we are given a periodic orbit of the modular flow. We wish to show that it corresponds to the conjugacy class of some hyperbolic element in $\mathrm{PSL}_2\mathbb{Z}$. The periodic orbit can be described by some $M \in \mathrm{PSL}_2\mathbb{R}$ and $t \in \mathbb{R}$ where $\delta_t M(\mathbb{Z}^2) = M(\mathbb{Z}^2)$. Observe that if $A = M^{-1}\delta_t M$, then

$$A(\mathbb{Z}^2) = M^{-1}\delta_t M(\mathbb{Z}^2) = M^{-1}M(\mathbb{Z}^2) = \mathbb{Z}^2.$$

Thus by Lemma 1.2, $A \in \mathrm{PSL}_2\mathbb{Z}$. Note, however, that our choice of M was not unique. Let $N \in \mathrm{PSL}_2\mathbb{R}$ be such that $M(\mathbb{Z}^2) = N(\mathbb{Z}^2)$. Then again by the lemma, we have that $N = MB$ for some $B \in \mathrm{PSL}_2\mathbb{Z}$, so

$$N^{-1}\delta_t N = (MB)^{-1}\delta_t(MB) = B^{-1}M^{-1}\delta_t MB = B^{-1}AB.$$

Hence every periodic orbit defines a conjugacy class of some element $A \in \mathrm{PSL}_2\mathbb{Z}$. We now show that A is hyperbolic by computing its trace directly. Since $MAM^{-1} = \delta_t$ and trace is invariant under conjugation, we have that

$$\begin{aligned} \mathrm{tr}(A) &= \mathrm{tr}(MAM^{-1}) \\ &= \mathrm{tr}(\delta_t) \\ &= e^t + e^{-t} \\ &= \left(\sum_{k=0}^{\infty} \frac{t^k}{k!} \right) + \left(\sum_{k=0}^{\infty} \frac{(-t)^k}{k!} \right) \\ &= \sum_{k=0}^{\infty} \frac{t^k + (-t)^k}{k!} \\ &= 2 + 0 + \frac{t^2 + t^2}{2!} + 0 + \frac{t^4 + t^4}{4!} + \dots \\ &> 2. \end{aligned}$$

Thus A is indeed hyperbolic. To summarize, there are two maps

$$\left\{ \begin{array}{l} \text{conjugacy classes of} \\ \text{hyperbolic } A \in \mathrm{PSL}_2\mathbb{Z} \end{array} \right\} \leftrightarrow \left\{ \begin{array}{l} \text{periodic orbits of} \\ \text{the modular flow} \end{array} \right\}$$

and it is straightforward to observe that they form a bijection. □

1.2 The Classical Perspective on the Modular Flow

Our construction of the modular flow is a non-standard take on a well-known and classically studied dynamical system called *the geodesic flow on the modular surface*. Here, we provide a brief sketch of the more classical construction of this system and then motivate the alternative perspective we have just detailed.

Let $\mathbb{H} = \{x + iy \in \mathbb{C} : y > 0, x, y \in \mathbb{R}\}$ be the upper half plane. There is an action of the **modular group** $\mathrm{PSL}_2\mathbb{Z} = \mathrm{SL}_2\mathbb{Z}/\{\pm I\}$ on \mathbb{H} defined by

$$\begin{aligned} \mathrm{PSL}_2\mathbb{Z} \times \mathbb{H} &\rightarrow \mathbb{H} \\ (\gamma, \tau) &\mapsto \gamma\tau = \frac{a\tau + b}{c\tau + d} \end{aligned}$$

where

$$\gamma = \begin{pmatrix} a & b \\ c & d \end{pmatrix} \in \mathrm{PSL}_2\mathbb{Z}.$$

Such a map is called a **linear fractional transform**. The **modular surface** \mathcal{M} is the quotient of \mathbb{H} by this action of $\mathrm{PSL}_2\mathbb{Z}$. More explicitly, \mathcal{M} is the set of all orbits $\{\gamma\tau : \gamma \in \mathrm{PSL}_2\mathbb{Z}\}$ as τ varies over of \mathbb{H} . The subset

$$\mathcal{F} = \{\tau \in \mathbb{H} : |\mathrm{Re}(x)| \leq 1/2, |\tau| \geq 1\}$$

of \mathbb{H} contains exactly one point from each one of these orbits (except on its boundary), and thus provides a convenient geometrical region that represents the modular surface (the region \mathcal{F} is a **fundamental domain** for \mathcal{M}). The right and left vertical boundary of \mathcal{F} are identified by the action of $\mathrm{PSL}_2\mathbb{Z}$, as well as the right and left bottom circular boundary. In Figure 1.3, we visualize \mathcal{F} along with its image under several elements of $\mathrm{PSL}_2\mathbb{Z}$. For a more thorough treatment of \mathbb{H} , $\mathrm{PSL}_2\mathbb{Z}$, and \mathcal{F} , see [Kat92].

Recall that an **n -dimensional manifold** is a generalization of n -dimensional Euclidean space; some small neighborhood of every point on a manifold looks like n -dimensional Euclidean space. A **Riemannian manifold** is a smooth and real man-

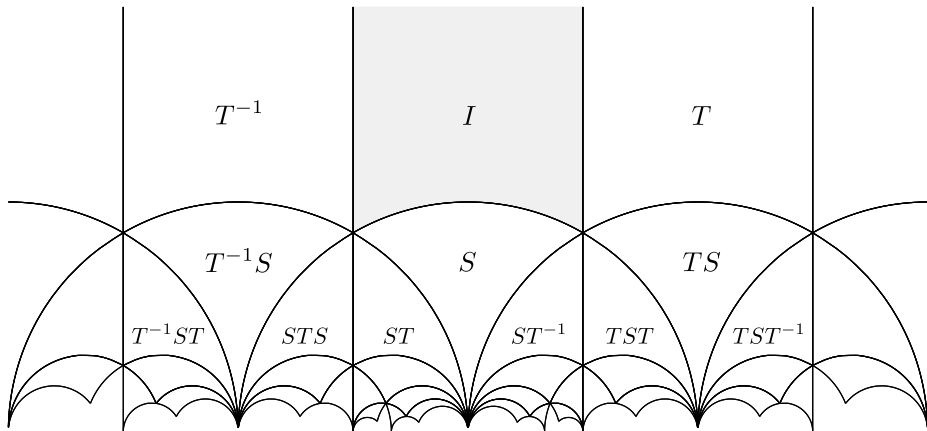
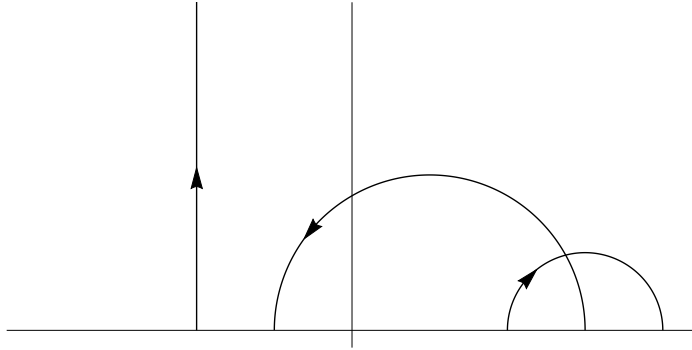


Figure 1.3: The elements of \mathcal{M} are orbits of \mathbb{H} under the action of $\mathrm{PSL}_2\mathbb{Z}$. Every orbit has exactly one representative in the shaded region \mathcal{F} . The image of \mathcal{F} by various elements of the modular group (in terms of the modular group generators S and T) are shown alongside \mathcal{F} . These translates are called **faces** in a **tessellation** of \mathbb{H} by its fundamental domain.

Figure 1.4: Example geodesics in \mathbb{H} .

ifold M equipped with an Riemannian inner product on the tangent space $T_p M$ for each point p in M . A **geodesic path** is the generalization of a straight line in Euclidean space to Riemannian manifolds—the quickest way between two points across the surface of a manifold is via a geodesic path, just as the quickest way between two points in Euclidean space is via a straight line. The prototypical example of a geodesic is a curved arc across the surface of the 2-sphere. In \mathbb{H} , geodesics under the Poincaré metric

$$ds = \frac{\sqrt{dx^2 + dy^2}}{y},$$

consist of straight vertical lines originating at the x -axis, and half-circles that meet the x -axis at right angles (see Figure 1.4).

Now, suppose that M is a Riemannian manifold. Given a point $p \in M$ and a direction v in the space tangent to M at p , the **geodesic flow on M** through p in the direction of v can be simply described as the flow along the geodesic in M that points in the direction of v . A **closed orbit of the geodesic flow** is a geodesic that returns to its initial position pointing in the same initial direction v .

The physical interpretation of the geodesic flow is to think of a particle moving on a manifold M subject to no constraints other than that it must stay on M . Many fundamental equations in physics, such as the Euler equations of motion of a rigid body or the Euler equations of fluid dynamics of an inviscid incompressible fluid, are examples of the geodesic flow on particular manifolds [Arn66; Tao10].

For Riemannian manifolds, one may also define the unit tangent bundle. The **unit tangent bundle $UT(M)$ of a manifold M** consists of pairs (p, v) , where $p \in M$ and v is a unit tangent vector to M at p . There exists a natural projection $\pi : (p, v) \mapsto p$ mapping $UT(M)$ onto M .

The space of nontrivial lattices up to homothety \mathcal{L}_1 is isomorphic to the unit tangent bundle for the modular surface \mathcal{M} . Thus every lattice $L \in \mathcal{L}_1$ implicitly describes a point in \mathcal{M} and a unit tangent direction—all the data needed to define the geodesic

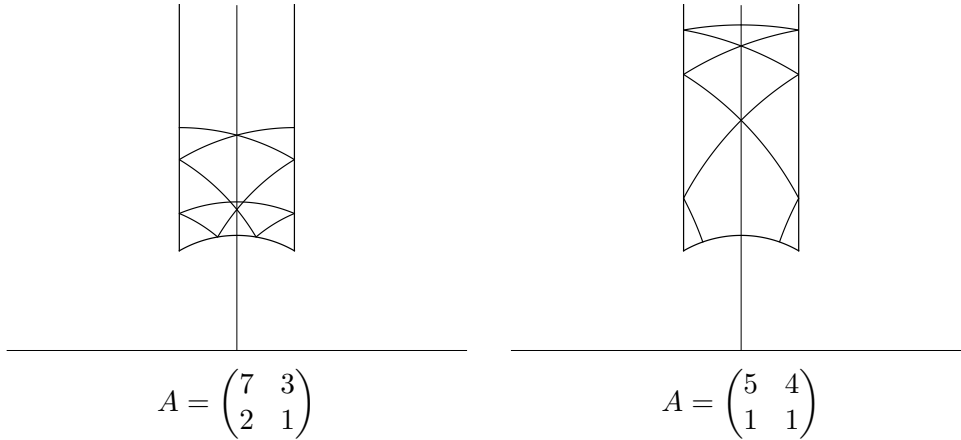


Figure 1.5: Periodic orbits of modular flow corresponding to matrices $A \in \mathrm{PSL}_2\mathbb{Z}$, projected down into \mathcal{M} and visualized in the fundamental domain \mathcal{F} . In \mathcal{F} , the right and left vertical boundaries are identified, and the right and left bottom circular boundaries are identified.

flow on \mathcal{M} . When we study the “modular flow”, we are really studying the lift of the geodesic flow on \mathcal{M} into the tangent space $\mathrm{UT}(M)$. If we project an orbit of the modular flow back down into \mathcal{M} , we recover a (rescaled) orbit of the geodesic flow on \mathcal{M} .

Suppose $L \in \mathcal{L}_1$ is a lattice generated by ω_1 and ω_2 such that $\omega_1, \omega_2 \in \mathbb{H}$ and the angle between ω_1 and ω_2 is positive and less than 180 degrees. Then the map $L \mapsto \omega_1/\omega_2$ is a projection from $\mathcal{L}_1 = \mathrm{UT}(\mathcal{M})$ to \mathcal{M} (see [Sil94, pp. 6-13]). The projection onto \mathcal{M} of several orbits of the modular flow in \mathcal{L}_1 are visualized in Figure 1.5.

The idea to consider a lift of the geodesic flow on \mathcal{M} rather than the geodesic flow on \mathcal{M} itself is a recent and novel contribution from Ghys in [Ghy07]. In addition to being homeomorphic to \mathcal{L}_1 , the unit tangent bundle of \mathcal{M} is homeomorphic to the knot complement of the trefoil knot $S^3 \setminus K$, as we shall see in Section 2.2. Thus Ghys studies the periodic orbits of the geodesic flow *as knots*, and obtains an interesting result relating a simple algebraic invariant of these knots back to the modular group $\mathrm{PSL}_2\mathbb{Z}$. We summarize this result in Section 2.3. A third space, $\exp_{\{2,3\}} S^1$, is homeomorphic to the unit tangent bundle of \mathcal{M} as well. In Chapter 3, we use this third space to analyze homotopy classes of periodic orbits in each space homeomorphic to the unit tangent bundle.

To summarize, the rest of this document is concerned with the modular flow in the upper row of the following diagram:

$$\begin{array}{ccccc} \exp_{\{2,3\}} S^1 & \xleftarrow{\cong} & \mathcal{L}_1 & \xleftarrow{\cong} & S^3 \setminus K \\ & & \downarrow \pi & & \\ & & \mathcal{M} & & \end{array}$$

Chapter 2

The 3-sphere and the Trefoil Complement

2.1 The Fundamental Group of the Trefoil Complement

The **3-sphere** is the set of complex tuples

$$S^3 = \{(u, v) \in \mathbb{C}^2 : |u|^2 + |v|^2 = 1\}$$

This set is endowed with the usual subspace topology, and is commonly employed in the study of knots or links. Technically speaking, we say that a **knot** is an embedding $S^1 \hookrightarrow S^3$, considered up to isotopy. Intuitively, a knot is a loop in 3-space with interesting twisting behavior and no self-intersections.

In our case, we're interested in a particular prototypical knot called the **trefoil** (visualized in Figure 2.1). This is the knot that, when laid on the surface of the torus, crosses the meridian of the torus three times and crosses longitudinal circles twice—as such it is also known as the **(2, 3)-torus knot**.

For any knot $K : S^1 \hookrightarrow S^3$, we can study the **knot complement** space $S^3 \setminus K$. Historically, such spaces have provided useful knot invariants via their fundamental group and interesting examples of 3-manifolds. The fundamental group of the trefoil complement happens to be isomorphic to a famous group with a convenient physical interpretation, which we will describe shortly. First, we recall the definition of a fundamental group as well as a useful theorem for computing fundamental groups.

Definition 2.1. Let X be a topological space. A **loop in X based at p** is a continuous map $f : I \rightarrow X$ such that $f(0) = f(1) = p$. Two loops f and g based at p are **path-homotopic** if there exists a continuous map $H : I \times I \rightarrow X$ such that

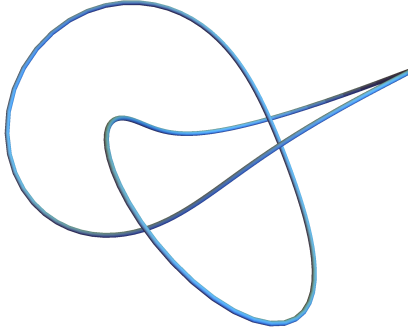


Figure 2.1: A trefoil knot. While the knot is embedded inside S^3 , we can stereographically project S^3 to \mathbb{R}^3 for visualization purposes.

for all s and t in I , $H(s, 0) = f(s)$, $H(s, 1) = g(s)$, and $H(0, t) = H(1, t) = p$. The path-homotopy relation is an equivalence relation on the set of all loops in X based at p , and we call the equivalence class of a loop its **path class**. The **fundamental group of X based at p** is the set of path classes of loops in X based at p , denoted $\pi_1(X, p)$. The set $\pi_1(X, p)$ forms a group under the operation of path composition.

Morally, two loops in X are homotopic if they can be continuously deformed into one another. The fundamental group describes the group structure of all based loops in X up to homotopy.

There is no general method for computing the fundamental group of an arbitrary topological space. Instead, we rely on a toolkit of methods and theorems that prove useful in different situations. One essential such tool is the Seifert Van-Kampen theorem.

Definition 2.2. Let H , G_1 , and G_2 be groups with presentations

$$\begin{aligned} G_1 &\cong \langle \alpha_1, \dots, \alpha_m : \rho_1, \dots, \rho_r \rangle, \\ G_2 &\cong \langle \beta_1, \dots, \beta_n : \sigma_1, \dots, \sigma_s \rangle, \text{ and} \\ H &\cong \langle \gamma_1, \dots, \gamma_p : \tau_1, \dots, \tau_t \rangle. \end{aligned}$$

Then if $f_1 : H \rightarrow G_1$ and $f_2 : H \rightarrow G_2$ are group homomorphisms, the **amalgamated free product** of G_1 and G_2 along H is the group with presentation

$$\begin{aligned} G_1 *_H G_2 &\cong \langle \alpha_1, \dots, \alpha_m, \beta_1, \dots, \beta_n : \rho_1, \dots, \rho_r, \\ &\quad \sigma_1, \dots, \sigma_s, u_1 = v_1, \dots, u_p = v_p \rangle \end{aligned}$$

where u_a is an expression for $f_1(\gamma_a) \in G_1$ in terms of the generators $\{\alpha_i\}$ and v_a similarly expresses $f_2(\gamma_a) \in G_2$ in terms of $\{\beta_j\}$.

Theorem 2.3 (Seifert-van Kampen Theorem). Let X be a topological space, and suppose that $X = U_1 \cup U_2$ for two open and path-connected subsets $U_1, U_2 \subseteq X$. In addition, suppose that $U_1 \cap U_2$ is path-connected and nonempty, and let $p \in U_1 \cap U_2$. There exists an isomorphism

$$\Phi : \pi_1(U_1, p) *_{\pi_1(U_1 \cap U_2, p)} \pi_2(U_2, p) \rightarrow \pi_1(X, p)$$

such that the following diagram commutes:

$$\begin{array}{ccccc} & i_1 & \nearrow & j_1 & \\ \pi_1(U_1 \cap U_2) & \swarrow & \downarrow & \searrow & \pi_1(X) \\ & \pi_1(U_1) *_{\pi_1(U_1 \cap U_2)} \pi_2(U_2) & \dashrightarrow^{\Phi} & & \\ & i_2 & \uparrow & j_2 & \end{array}$$

Now, we provide an explicit computation of the fundamental group of the trefoil complement. For additional details, see [Hat02, pp. 47–49] and [Sti93, pp. 153–154].

Proposition 2.4. Let K be the trefoil knot. Then

$$\pi_1(S^3 \setminus K) = \langle x, y : x^2 = y^3 \rangle$$

Proof. We proceed by two applications of the Seifert-van Kampen theorem. First we compute $\pi_1(\mathbb{R}^3 \setminus K)$, since it is slightly easier to compute than $\pi_1(S^3 \setminus K)$.

Let $T \subset \mathbb{R}^3 \setminus K$ be the solid torus with K removed and N be a thin tubular neighborhood of K . Let $X = T \setminus N$ and $Y = (\mathbb{R}^3 \setminus T) \setminus N$. Then X and Y meet at a region L that looks like the surface of the solid torus with N removed. As shown in Figure 2.2, L is an annulus.

Since L is an annulus, its fundamental group is infinite cyclic with a single generator ℓ . The space X is a solid torus with a neighborhood of the trefoil removed, which deformation retracts onto a circle. So $\pi_1(X)$ is infinite cyclic as well, with generator x corresponding to the loop around the axis of the solid torus. In X , the generator ℓ is a trefoil loop around the torus that crosses longitudinal circles twice, so we have

$$\ell \simeq x^2.$$

The fundamental group of Y is also infinite cyclic, with the generator y corresponding to a loop that “links” the hole of the solid torus. The loop ℓ crosses meridian circles in the solid torus three times, so we have that

$$\ell \simeq y^3.$$

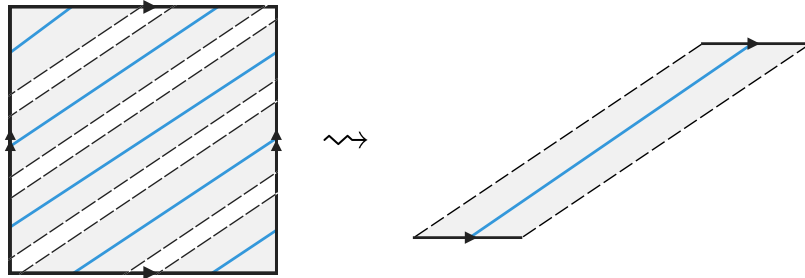


Figure 2.2: The region L is the torus with a thin tubular neighborhood of the trefoil N removed. Here, N is depicted in white and L is shaded in gray on the flat torus. While still respecting the appropriate edge identifications, the pieces of the torus can be rearranged to form an annulus. The generator ℓ of π_1 of this annulus is shown in blue.

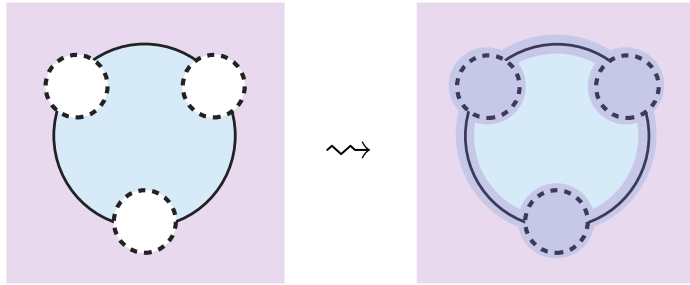


Figure 2.3: The picture on the left shows a longitudinal slice of the torus T , with the absence of tubular neighborhood N of the trefoil shown in white. The regions X and Y are depicted in blue and pink, respectively. On the right, X and Y have been expanded to X' and Y' , respectively.

Now, we can expand X and Y slightly to open sets $X' \supseteq X$ and $Y' \supseteq Y$ such that $X' \cap Y'$ is an open neighborhood of L and $X' \cup Y' = \mathbb{R}^3 \setminus K$ (see Figure 2.3). Then, applying Van Kampen, we have that

$$\pi_1(\mathbb{R}^3 \setminus K) = \langle x, y : x^2 = y^3 \rangle.$$

Now we show that $\pi_1(\mathbb{R}^3 \setminus K) = \pi_1(S^3 \setminus K)$ with another application of Van Kampen. Decompose $S^3 \setminus K$ into $(\mathbb{R}^3 \setminus K) \cup B$, where B is an open set containing the compactification point and the complement of a large closed ball containing K . Both B and $B \cap (\mathbb{R}^3 \setminus K)$ are simply connected. By Van Kampen, the inclusion $\mathbb{R}^3 \setminus K \hookrightarrow S^3 \setminus K$ induces an isomorphism of groups

$$\Phi : \pi_1(\mathbb{R}^3 \setminus K,) \rightarrow \pi_1(S^3 \setminus K)$$

as shown by the following commutative diagram:

$$\begin{array}{ccccc}
 & & \pi_1(\mathbb{R}^3 \setminus K) & & \\
 & \searrow & \downarrow & \nearrow & \\
 \pi_1(B \cap (\mathbb{R}^3 \setminus K)) & & \pi_1(B) * \pi_1(\mathbb{R}^3 \setminus K) & \xrightarrow{\Phi} & \pi_1(S^3 \setminus K) \\
 & \swarrow & \uparrow & & \nearrow \\
 & 1 & & & 1
 \end{array}$$

Thus we have the desired result. \square

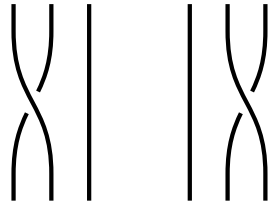
The fundamental group of the trefoil complement is isomorphic to a well-known group, the **braid group on 3 strands**. This group has presentation

$$B_3 = \langle \sigma_1, \sigma_2 : \sigma_1 \sigma_2 \sigma_1 = \sigma_2 \sigma_1 \sigma_2 \rangle.$$

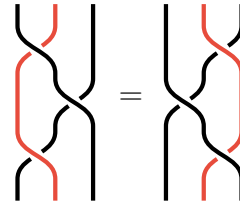
The isomorphism $\pi_1(S^3 \setminus K) \rightarrow B_3$ is given by sending generators

$$\begin{aligned}
 x &\mapsto \sigma_0 \sigma_1 \sigma_0 \\
 y &\mapsto \sigma_0 \sigma_1
 \end{aligned} \tag{2.1}$$

This group appears in many different contexts: it is the mapping class group of the thrice-punctured disk, the universal central extension of $\mathrm{PSL}_2 \mathbb{Z}$, and so forth. It also has a convenient visual interpretation, where the generators σ_1 and σ_2 are depicted and composed as in Figure 2.4. We will return to this visual interpretation in Chapter 3, where we decompose the path class of various loops in $\exp_{\{2,3\}} S^1 \cong S^3 \setminus K$ as visual generators of B_3 .



(a) The generators σ_1 and σ_2 of B_3



(b) The single relation in B_3 , known as the **third Reidemeister move**.

Figure 2.4: The visual interpretation of B_3 , where each generator is thought of as a braiding of three strands of string that start and end at fixed points. The group operation corresponds to stacking the visual generators top to bottom to compose a more complex braiding of string. The single relation in B_3 can be thought of as “pulling a string” without moving the endpoints, which preserves the isotopy class of the braid.

2.2 From \mathcal{L} to S^3

At first glance, the space of two-dimensional lattices up to homothety and the three-dimensional sphere may seem quite different. It turns out that they are indeed homeomorphic. We now describe an explicit homeomorphism $\mathcal{L} \rightarrow S^3$ as sketched by Mostovoy in [Mos04].

Let $L \in \mathcal{L}$ and $k \in \mathbb{Z}$. Define

$$G_k(L) = \sum_{\omega \in L, \omega \neq 0} \omega^{-k}.$$

When $k \geq 4$, this series converges and is known as an **Eisenstein series**. For nondegenerate L , these numbers are the parameters in the Weierstrass \wp_L -function identity

$$(\wp'_L)^2 = 4\wp_L^3 - 60G_4(L)\wp_L - 140G_6(L).$$

The following facts about $G_4(L)$ and $G_6(L)$ are fundamental to the theory of elliptic functions:

- (i) For $t > 0$ and any L , $G_4(tL) = t^{-4}G_4(L)$ and $G_6(tL) = t^{-6}G_6(L)$ [AS64, p. 631].
- (ii) The map $L \mapsto (G_4(L), G_6(L))$ is a homeomorphism $\mathcal{L} \rightarrow \mathbb{C}^2 \setminus \{0\}$ [Ser73, pp. 82, 89].
- (iii) A tuple $(u, v) \in \mathbb{C}^2 \setminus \{0\}$ is the image of a degenerate lattice under this map if and only if $20u^3 - 49v^2 = 0$ [Ghy07, p. 265].

Thus for any nontrivial lattice L , we can obtain a unique rescaling $L' = tL$ for some $t > 0$ such that

$$|G_4(L')|^2 + |G_6(L')|^2 = 1$$

Then the map $L \mapsto (G_4(L'), G_6(L'))$ lands in S^3 , and we have the desired homeomorphism $\mathcal{L} \rightarrow S^3$.

The image of the degenerate lattices under this map is the intersection of the curve $20u^3 - 49v^2 = 0$ with the 3-sphere. For any $a \in \mathbb{R}$, it happens that the intersection of complex curve $u^3 + av^2 = 0$ with the 3-sphere is a trefoil knot [Mil68, p. 4]. Thus, the image of degenerate lattices under the homeomorphism is the trefoil shown in Figure 2.1.

2.3 The Linking Number of Periodic Orbits in S^3

We have observed the periodic orbits of the modular flow in the space of lattices in Section 1.1, and we have just seen that the space of lattices is homeomorphic to the 3-sphere. It is now natural to ask: how do these periodic orbits present in the 3-sphere?

The degenerate lattices are sent to the trefoil knot in the 3-sphere, but the periodic orbits of this flow exist entirely within the space of nondegenerate lattices. Thus we can say that in the 3-sphere, a periodic orbit of the modular flow in the space of lattices determines a link with the trefoil knot. Since each periodic flow is associated with some hyperbolic $A \in \mathrm{PSL}_2\mathbb{Z}$ we call the corresponding trefoil link k_A a **modular trefoil link** or **modular knot**, following after [Ghy07]. Several examples of such links are shown in Figure 2.5.

The periodic orbits of the modular flow provide a rich variety of trefoil links. One classically studied invariant of two-component links is their **linking number**, an integer associated with a particular link. The linking number of a two-component link can be defined computationally as follows:

1. Color the components of the link red and blue, respectively, and give each component an orientation.
2. Project the colored, oriented link onto the plane. Any regular projection will do.
3. Assign each crossing of a red strand over blue strand a number, either 1 or -1 according to the diagram in Figure 2.6.
4. Sum the integers at all crossings to obtain the linking number.

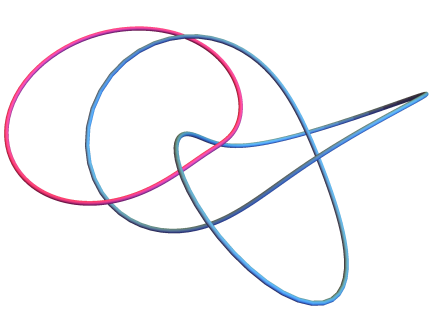
A simple example is shown in Figure 2.7. For a more complex example, consider the first link in Figure 2.5; it has linking number 0.

In [Ghy07], Ghys proves a fascinating result relating the linking numbers of modular trefoil links to a famous arithmetic function. To understand this function and subsequent result, we first need to understand a few facts about $\mathrm{SL}_2\mathbb{Z}$ and its relative, $\mathrm{PSL}_2\mathbb{Z}$.

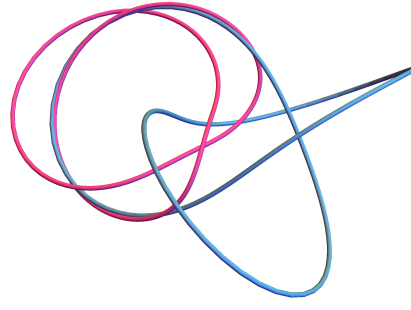
First, we will look at the basic building block of each group—their generators.

Proposition 2.5. The group $\mathrm{SL}_2\mathbb{Z}$ is generated by the matrices

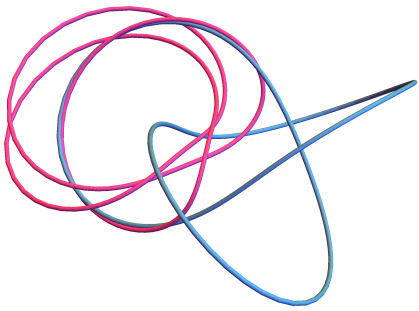
$$S = \begin{pmatrix} 0 & -1 \\ 1 & 0 \end{pmatrix}, \quad T = \begin{pmatrix} 1 & 1 \\ 0 & 1 \end{pmatrix}$$



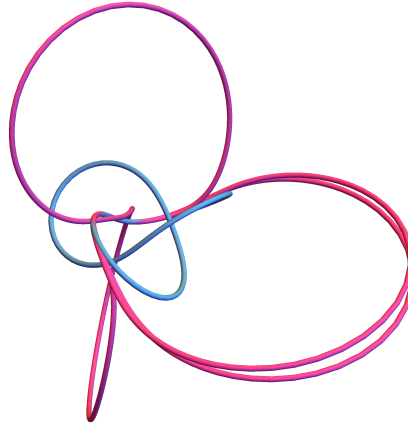
$$A = \begin{pmatrix} 1 & 1 \\ 1 & 2 \end{pmatrix}$$



$$A = \begin{pmatrix} 2 & 3 \\ 5 & 8 \end{pmatrix}$$



$$A = \begin{pmatrix} 13 & 8 \\ 21 & 13 \end{pmatrix}$$



$$A = \begin{pmatrix} 43 & 163 \\ 67 & 254 \end{pmatrix}$$

Figure 2.5: A matrix $A \in \mathrm{PSL}_2\mathbb{Z}$ determines a periodic orbit of a flow in \mathcal{L} , which in turn determines a modular trefoil link k_A in S^3 . Here, we visualize k_A for several values of A .

Proof. Let $\alpha \in \mathrm{SL}_2\mathbb{Z}$. First we show that there exists some $\gamma \in \langle S, T \rangle$ such that $\gamma\alpha$ is a matrix with lower left entry 0. Note that for all $n \in \mathbb{Z}$,

$$\begin{pmatrix} 1 & n \\ 0 & 1 \end{pmatrix} = \begin{pmatrix} 1 & 1 \\ 0 & 1 \end{pmatrix}^n = T^n \in \langle S, T \rangle$$

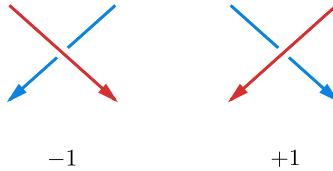


Figure 2.6: Diagrammatic rules for computing the linking number of link.

Then for any matrix $\begin{pmatrix} a & b \\ c & d \end{pmatrix}$, we have the identities

$$S \begin{pmatrix} a & b \\ c & d \end{pmatrix} = \begin{pmatrix} -c & -d \\ a & b \end{pmatrix}, \quad T^n \begin{pmatrix} a & b \\ c & d \end{pmatrix} = \begin{pmatrix} a + nc & b + nd \\ c & d \end{pmatrix}$$

Now, let $\alpha = \begin{pmatrix} a & b \\ c & d \end{pmatrix}$. If $c = 0$, then $\gamma = I$ and we are done. So suppose $c \neq 0$. If $|a| < |c|$, left multiply α by S . Then $|a| \geq |c|$, so we can divide a by c . Then we have $a = qc + r$ with $0 \leq r < |c|$. Then $T^{-q}\alpha$ has upper left entry $r = a - qc$, which has absolute value smaller than the lower left entry of $T^{-q}\alpha$. Applying S to $T^{-q}\alpha$ switches the upper and lower left entries, and we can apply the division algorithm again. After each iteration of this process, we obtain a matrix with lower left entry whose absolute value is strictly less than before. So eventually we have a word γ in S and T such that $\gamma\alpha$ has lower left entry 0. To summarize, at the end of the following algorithm we have a word γ in S and T such that $\gamma\alpha$ has lower-left entry 0.

```

 $\gamma \leftarrow I$ 
if  $(\gamma\alpha)_{0,0} > (\gamma\alpha)_{1,0}$  then  $\gamma \leftarrow S\gamma$ 
while  $(\gamma\alpha)_{1,0} \neq 0$  do
     $q \leftarrow a // c$ 
     $r \leftarrow a \% c$ 
     $\gamma \leftarrow T^{-q}\gamma$ 
    if  $(\gamma\alpha)_{0,0} > (\gamma\alpha)_{1,0}$  then  $\gamma \leftarrow S\gamma$ 

```

Since the determinant is multiplicative, $\gamma\alpha$ also has determinant 1. Hence $\gamma\alpha$ must be of the form $\begin{pmatrix} 1 & n \\ 0 & 1 \end{pmatrix}$ or $\begin{pmatrix} -1 & n \\ 0 & -1 \end{pmatrix}$ for some $n \in \mathbb{Z}$. So $\gamma\alpha = \pm T^n$, which means that $\alpha = \pm\gamma^{-1}T^n$. Both $\gamma^{-1}T^n$ and $-\gamma^{-1}T^n = -I\gamma^{-1}T^n = S^2\gamma^{-1}T^n$ are in $\langle S, T \rangle$. Thus we have taken an arbitrary $\alpha \in \text{SL}_2\mathbb{Z}$ and represented it as an element in $\langle S, T \rangle$, thus

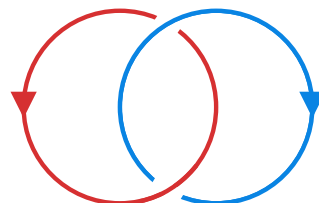


Figure 2.7: A simple link. The red component crosses over the blue component exactly once. According to Figure 2.6, this link has linking number 1.

$\mathrm{SL}_2\mathbb{Z} \subseteq \langle S, T \rangle$. The reverse inclusion is apparent. \square

Given the generators of a group, we can of course write down every element in the group as a word in those generators. We now describe more precisely the structure of elements of $\mathrm{PSL}_2\mathbb{Z}$ as generator words.

Lemma 2.6. The group $\mathrm{PSL}_2\mathbb{Z} = \langle S, T \rangle = \langle U, V \rangle = \langle P, Q \rangle$, where

$$U = \begin{pmatrix} 0 & 1 \\ -1 & 0 \end{pmatrix}, \quad V = \begin{pmatrix} 1 & -1 \\ 1 & 0 \end{pmatrix}, \quad P = \begin{pmatrix} 1 & 1 \\ 0 & 1 \end{pmatrix}, \quad Q = \begin{pmatrix} 1 & 0 \\ 1 & 1 \end{pmatrix}$$

and S and T are as before.

Proof. The group $\mathrm{PSL}_2\mathbb{Z}$ is all integer matrices A such that $\det A = 1$, subject to the identification $A = -A$. Since $\mathrm{SL}_2\mathbb{Z} = \langle S, T \rangle$ and any such A is in $\mathrm{SL}_2\mathbb{Z}$, we have that S and T generate $\mathrm{PSL}_2\mathbb{Z}$ as well. In $\mathrm{PSL}_2\mathbb{Z}$, we also have that $S = U = P^{-1}QP^{-1}$ and $T = VU = P$. Thus $\mathrm{PSL}_2\mathbb{Z} = \langle S, T \rangle = \langle U, V \rangle = \langle P, Q \rangle$. \square

Lemma 2.7. Any element of $\mathrm{PSL}_2\mathbb{Z}$ can be written in shortest form as

$$V^{\varepsilon_0}UV^{\varepsilon_1}U\dots V^{\varepsilon_n}UV^{\varepsilon_{n+1}} \tag{2.2}$$

where $\varepsilon_0, \varepsilon_{n+1} \in \{-1, 0, 1\}$ and $\varepsilon_i \in \{-1, 1\}$ for $1 \leq i \leq n$.

Proof. Let $A \in \mathrm{PSL}_2\mathbb{Z}$. Since $\mathrm{PSL}_2\mathbb{Z} = \langle U, V \rangle$, we have that A can be written in shortest form as

$$V^{\varepsilon_0}U^{\varepsilon_1}V^{\varepsilon_2}\dots U^{\varepsilon_n}V^{\varepsilon_{n+1}}$$

where $\varepsilon_i \neq 0$ for all $1 \leq i \leq n$. But we also have that

$$U^2 = V^3 = \begin{pmatrix} -1 & 0 \\ 0 & -1 \end{pmatrix} = I.$$

Thus $\varepsilon_i \in \mathbb{Z}/3\mathbb{Z}$ for all i , and $\varepsilon_i \not\equiv 0 \pmod{3}$ for $1 \leq i \leq n$. And since $V^2 = V^{-1}$, we have that

$$A = V^{\varepsilon_0}UV^{\varepsilon_1}U\dots V^{\varepsilon_n}UV^{\varepsilon_{n+1}}$$

where $\varepsilon_i = \pm 1$ for $1 \leq i \leq n$, the desired result. \square

The representation in (2.2) ends up being unique; for details see [Ran77, p. 12].

Now, recall that the hyperbolic elements of $\mathrm{PSL}_2\mathbb{Z}$ are those with trace greater than 2, and that we are interested in the hyperbolic elements because the conjugacy classes of hyperbolic elements are in bijection with the periodic orbits of the modular flow. A

result of Rademacher can help us say more about the generator words of hyperbolic elements in particular.

Lemma 2.8. Let $A, B \in \mathrm{PSL}_2\mathbb{Z}$. If $\mathrm{tr} A \neq \mathrm{tr} B$, then A is not conjugate to B .

Proof. Let

$$A = \begin{pmatrix} a_1 & a_2 \\ a_3 & a_4 \end{pmatrix}, \quad B = \begin{pmatrix} b_1 & b_2 \\ b_3 & b_4 \end{pmatrix}, \quad \text{and} \quad C = \begin{pmatrix} c_1 & c_2 \\ c_3 & c_4 \end{pmatrix}$$

be elements of $\mathrm{PSL}_2\mathbb{Z}$ such that $\mathrm{tr} A \neq \mathrm{tr} B$, and assume for the sake of contradiction that A is conjugate to B by C . Then

$$\begin{aligned} B &= CAC^{-1} \\ \implies \begin{pmatrix} b_1 & b_2 \\ b_3 & b_4 \end{pmatrix} &= \begin{pmatrix} c_1 & c_2 \\ c_3 & c_4 \end{pmatrix} \begin{pmatrix} a_1 & a_2 \\ a_3 & a_4 \end{pmatrix} \begin{pmatrix} c_4 & -c_2 \\ -c_3 & c_1 \end{pmatrix} \\ \implies b_1 + b_4 &= (a_1 + a_4)(c_1 c_4 - c_2 c_3) \\ \implies b_1 + b_4 &= (a_1 + a_4) \det(C) \\ \implies b_1 + b_4 &= (a_1 + a_4) \\ \implies \mathrm{tr} B &= \mathrm{tr} A. \end{aligned}$$

Thus we have a contradiction, and so A is not conjugate to B . \square

Proposition 2.9 (Rademacher). Let $A \in \mathrm{PSL}_2\mathbb{Z}$. The conjugacy class of A has a shortest representative either of the form

$$U, V, \text{ or } V^{-1} \tag{2.3}$$

or of the form

$$UV^{\varepsilon_1}UV^{\varepsilon_2}\dots V^{\varepsilon_n} \tag{2.4}$$

where $\varepsilon_i \in \{-1, 1\}$ for $1 \leq i \leq n$. Any cyclic permutation of the factors in such a representation remains in the same conjugacy class, thus these representatives are considered only up to cyclic permutation. We call the form (2.4) a **UV decomposition of the conjugacy class of A** .

Proof. See [RG72, pp. 56–57]. \square

By Lemma 2.8, we know that any conjugacy class of a hyperbolic element in $\mathrm{PSL}_2\mathbb{Z}$ has a UV decomposition. Since $\mathrm{PSL}_2\mathbb{Z} = \langle U, V \rangle = \langle P, Q \rangle$, we can decompose elements of $\mathrm{PSL}_2\mathbb{Z}$ using P and Q instead, which ends up being slightly neater.

Corollary 2.10. Let $A \in \mathrm{PSL}_2\mathbb{Z}$ be conjugate to a matrix

$$M = UV^{\varepsilon_1}UV^{\varepsilon_2}\dots UV^{\varepsilon_n}$$

where $\varepsilon_i \in \{-1, 1\}$ for $1 \leq i \leq n$. Then A is conjugate to the word in P and Q where P replaces all occurrences of UV^1 and Q replaces all occurrences of UV^{-1} in M . This word is called a **PQ decomposition of the conjugacy class of A** .

Proof. One can check that

$$UV = P^{-1}QPQ^{-1}P \tag{2.5}$$

$$UV^{-1} = P^{-1}QP^{-1}P^{-1}QP^{-1}P^{-1} \tag{2.6}$$

and also that

$$P = U(P^{-1}QPQ^{-1}P)U^{-1} \tag{2.7}$$

$$Q = U(P^{-1}QP^{-1}P^{-1}QP^{-1}P^{-1})U^{-1}. \tag{2.8}$$

Let w_i be the PQ word in either (2.5) or (2.6), depending on whether ε_i is 1 or -1 , respectively. Then

$$UV^{\varepsilon_1}UV^{\varepsilon_2}\cdots UV^{\varepsilon_n} = w_1w_2\cdots w_n = w_1U^{-1}Uw_2U^{-1}U\cdots w_{n-1}U^{-1}Uw_n,$$

which is conjugate to a matrix

$$U(w_1U^{-1}Uw_2U^{-1}U\cdots w_{n-1}U^{-1}Uw_n)U^{-1} = (Uw_1U^{-1})(Uw_2U^{-1})\cdots(Uw_nU^{-1}).$$

Then by (2.7) and (2.8), this matrix is equivalent to replacing all UV with P and all UV^{-1} with Q in the expression $UV^{\varepsilon_1}UV^{\varepsilon_2}\cdots UV^{\varepsilon_n}$. \square

Note that any word in P and Q with P and Q each occurring at least once is a hyperbolic element in $\mathrm{PSL}_2\mathbb{Z}$. Shortly we will see that writing a hyperbolic element A as a PQ word provides insight into the periodic orbit that A defines. First, however, we need to understand the connection between $\mathrm{PSL}_2\mathbb{Z}$ and a classic arithmetic object we call the Rademacher class function. The building block of this function is an infinite series with a rather esoteric summand.

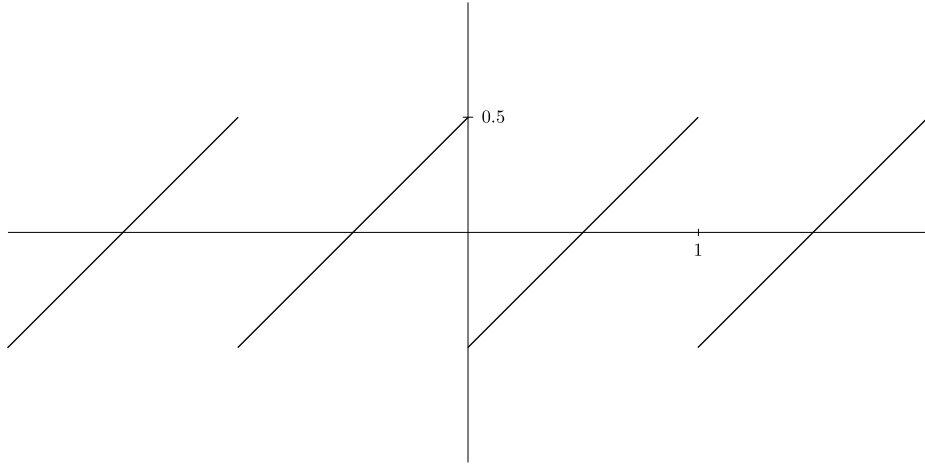
Definition 2.11. Let h and k be coprime integers with $k \geq 1$. The **Dedekind sum** $s(h, k)$ is the function given by

$$s(h, k) = \sum_{r=1}^k \left(\left(\frac{hr}{k} \right) \right) \left(\left(\frac{r}{k} \right) \right)$$

where the “sawtooth” function $((x))$ is defined as

$$((x)) = \begin{cases} x - \lfloor x \rfloor - 1/2 & \text{if } x \notin \mathbb{Z} \\ 0 & \text{if } x \in \mathbb{Z} \end{cases}$$

and $\lfloor x \rfloor$ is the floor of x . A graph of $((x))$ is shown in Figure 2.8

Figure 2.8: The sawtooth function $((x))$ for $-2 \leq x \leq 2$.

Definition 2.12. The **Rademacher function** $\Phi : \mathrm{PSL}_2\mathbb{Z} \rightarrow \mathbb{Z}$ is given by

$$\Phi \begin{pmatrix} a & b \\ c & d \end{pmatrix} = \begin{cases} b/d & \text{for } c = 0 \\ \frac{a+d}{c} - 12(\text{sign } c) s(d, |c|) & \text{for } c \neq 0 \end{cases}$$

The closely related **Rademacher class function** $\Psi : \mathrm{PSL}_2\mathbb{Z} \rightarrow \mathbb{Z}$ is defined as

$$\Psi \begin{pmatrix} a & b \\ c & d \end{pmatrix} = \Phi \begin{pmatrix} a & b \\ c & d \end{pmatrix} - 3 \text{sign}(c(a+d))$$

These functions appear rather intricate when taken by their direct definition. More often though, we are interested in certain properties of these functions instead.

Proposition 2.13 (Rademacher). Suppose $A, B \in \mathrm{PSL}_2\mathbb{Z}$ and let c_M be the lower left entry of any matrix M . Then

$$\Phi(AB) = \Phi(A) + \Phi(B) - 3 \text{sign}(c_A c_B c_{AB})$$

and

$$\Psi(AB) = \Psi(A) + \Psi(B)$$

Proof. Given in [Rad56]. □

It is perhaps surprising that a function built out of such intractable objects such as Dedekind sums splits nicely over addition. Indeed, the behavior of the Rademacher class function with respect to a UV decomposition of its parameter $A \in \mathrm{PSL}_2\mathbb{Z}$ is even more surprising.

Proposition 2.14 (Rademacher). Suppose that $A \in \mathrm{PSL}_2\mathbb{Z}$ is conjugate to a matrix of the form (2.4), say $A \sim UV^{\varepsilon_1}UV^{\varepsilon_2}\dots V^{\varepsilon_n}$. Then

$$\Psi(A) = \sum_{i=1}^n \varepsilon_i$$

In particular, Ψ is constant on conjugacy classes.

Proof. See [RG72, pp. 58-60]. \square

Corollary 2.15. Let $P^{i_1}Q^{j_1}\dots P^{i_n}Q^{j_m}$ be a PQ decomposition of the conjugacy class of $A \in \mathrm{PSL}_2\mathbb{Z}$. Then

$$\Psi(A) = \sum_{k=1}^n j_k - i_k$$

Proof. This follows from Proposition 2.14 in light of Corollary 2.10. \square

Finally, we are ready to understand a main result from Ghys on the periodic orbits of the modular flow.

Theorem 2.16 (Ghys). The linking number of a modular trefoil knot k_A is $\Psi(A)$.

To appreciate this remarkable fact, let's compute the linking number of the modular trefoil link k_A for

$$A = \begin{pmatrix} 32 & 25 \\ 23 & 18 \end{pmatrix}$$

The link k_A is rather intricate, as shown in Figure 2.9. While we could count colored crossings in this figure to obtain the linking number, we now have a much simpler method of computation. As a PQ word, $A = PQQPQPPPQ$. Then according to Corollary 2.15 and Theorem 2.16, the linking number of k_A is the number of P s minus the number of Q s in this PQ -decomposition of A . Thus, the linking number of k_A is $5 - 4 = 1$.

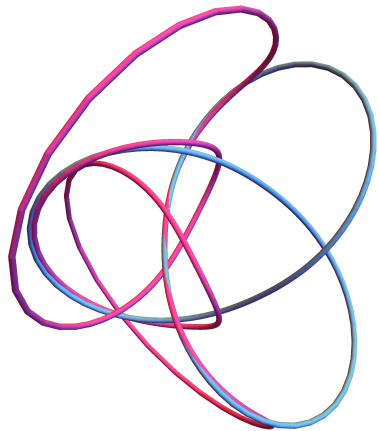


Figure 2.9: The modular trefoil link k_A for $A = \begin{pmatrix} 32 & 25 \\ 23 & 18 \end{pmatrix}$.

Chapter 3

Finite Subsets of the Circle

3.1 Topologizing $\exp_k X$

We now arrive at our third homeomorphic space, the set of all nonempty subsets of S^1 with at most 3 points. In general, we denote the set of all nonempty subsets with at most k points of a space X as $\exp_k X$, and refer to it as a **finite subset space**. Such a space can be given the topology induced by the quotient map

$$q : X^k \rightarrow \exp_k X$$
$$q(x_1, x_2, \dots, x_k) = \{x_1, x_2, \dots, x_k\}$$

Alternatively, if the underlying space X has metric structure, we can topologize $\exp_k X$ via an induced metric on subsets of X . Let d be a metric on X , and define the **r -inflation of $A \subseteq X$** as

$$A_r = \bigcup_{a \in A} \{x \in X : d(a, x) < r\}$$

Then the **Hausdorff distance** d_H between two subsets A and B of X is given by

$$d_H(A, B) = \inf \{\varepsilon \geq 0 : A \subseteq B_\varepsilon, B \subseteq A_\varepsilon\}$$

Intuitively, the Hausdorff distance between two subsets is the smallest amount they must be “inflated” in order to contain each other. The **Hausdorff metric topology** on $\exp_k X$ is the topology generated by the Hausdorff distance.

The Hausdorff metric topology provides a more instinctual notion of open sets in $\exp_k X$ than the above quotient topology, but results in literature concerning $\exp_k X$ often assume the quotient topology (which has the merit of not requiring additional metric structure on X). For X a metric space, however, it turns out that these two topologies are equivalent. Since results in literature concerning $\exp_k X$ are sparse in

general, we provide explicit proof of this fact.

Proposition 3.1. Let (X, d) be a metric space. The Hausdorff metric topology \mathcal{T}_H on X is equivalent to the quotient topology \mathcal{T}_q under the quotient map q .

Proof. To show that $\mathcal{T}_H \subseteq \mathcal{T}_q$, we will show that an arbitrary basis element for \mathcal{T}_H is in \mathcal{T}_q . Since \mathcal{T}_H is the metric topology generated by d_H , the set of all open balls in the metric d_H is a basis for \mathcal{T}_H . Let $A = \{a_1, a_2, \dots, a_\ell\} \in \exp_k X$ and $r > 0$ a real number, so that $B(A, r)$ is an arbitrary open ball in \mathcal{T}_H . We claim that

$$q^{-1}(B(A, r)) = \bigcup_{\substack{x=(x_1, \dots, x_k) \\ \in q^{-1}(B(A, r))}} B_d(x_1, r - r_x) \times \cdots \times B_d(x_k, r - r_x) \quad (3.1)$$

where

$$r_x = \max\{d(x_i, a_j) : 1 \leq i \leq k, 1 \leq j \leq \ell\}$$

Let $y = (y_1, \dots, y_k)$ be a point in the right-hand side of (3.1), so that $y \in \prod_i B_d(z_i, r - r_z)$ for some $z = (z_1, \dots, z_k)$, and let $q(y)_r$ and A_r be the r -inflation of $q(y)$ and A , respectively. Since each y_i is in $B_d(z_i, r - r_z)$, we have that $d(y_i, z_i) < r - r_z$. And for all z_i there exists some $a_j \in A$ such that $d(z_i, a_j) < r_z$ (by construction of r_z). Then by the triangle inequality,

$$d(y_i, a_j) \leq d(y_i, z_i) + d(z_i, a_j) < r - r_z + r_z = r$$

Thus $A \subseteq q(y)_r$. It can be shown similarly that $q(y) \subseteq A_r$ as well. It follows that $d_H(A, q(y)) < r$, hence $q(y) \in B(A, r)$ and $y \in q^{-1}(B(A, r))$.

Conversely, if $y \in q^{-1}(B(A, r))$, then it is clear that y is in the union containing products of balls centered at the coordinates of y . So (3.1) is verified.

Then we have that $q^{-1}(B(A, r))$ is a union of finite products of open sets in X , and so $q^{-1}(B(A, r))$ is open in X^k . Thus we have that \mathcal{T}_H is coarser than \mathcal{T}_q .

Now we will show that $\mathcal{T}_q \subseteq \mathcal{T}_H$ as well. Let $U \in \mathcal{U} \in \mathcal{T}_q$, and suppose that

$$(x_1, \dots, x_k) \in q^{-1}(U) \subseteq q^{-1}(\mathcal{U})$$

Since $q^{-1}(\mathcal{U})$ is open in X^k , we have that

$$q^{-1}(\mathcal{U}) = \bigcup_{j \in J} V_{j_1} \times \cdots \times V_{j_k}$$

for some index set J , where each V_{j_i} is open in (X, d) . Then $(x_1, \dots, x_k) \in V_{j_1} \times \cdots \times V_{j_k}$ for some $j \in J$. Since all V_{j_i} are open in (X, d) , for each x_i and some

corresponding radius r_i we can draw an open ball $B(x_i, r_i) \subseteq V_{j_i}$. So we have that

$$(x_1, \dots, x_k) \subseteq \prod_i B_d(x_i, r_i) \subseteq \prod_i V_{j_i}$$

Let $r = \min_i\{r_i\}$. We claim that $B(U, r) \subseteq \mathcal{U}$: if it weren't, then there would exist some $W \in B(U, r)$ that is not in \mathcal{U} . But then there would exist some $w \in q^{-1}(W)$ such that $w \in \prod_i B_d(x_i, r_i)$ and $w \notin q^{-1}(\mathcal{U})$. This is a contradiction, since $\prod_i B_d(x_i, r_i) \subseteq q^{-1}(\mathcal{U})$. Thus we have that $B(U, r) \subseteq \mathcal{U}$. Since $U \in \mathcal{U}$ was arbitrary, this means that \mathcal{U} is open in $(\exp_k X, \mathcal{T}_H)$, hence $\mathcal{T}_q \subseteq \mathcal{T}_H$. \square

3.2 From \mathcal{L} to $\exp_3 S^1$

For our purposes, we will focus on a particular finite subset space, $\exp_3 S^1$. In [Mos04], Mostovoy provides a homeomorphism $f : \mathcal{L} \rightarrow \exp_3 S^1$, which we now describe.

The **Voronoi cell** $V(L)$ of a nondegenerate lattice L is the cell in a Voronoi partition of L containing 0. As a set,

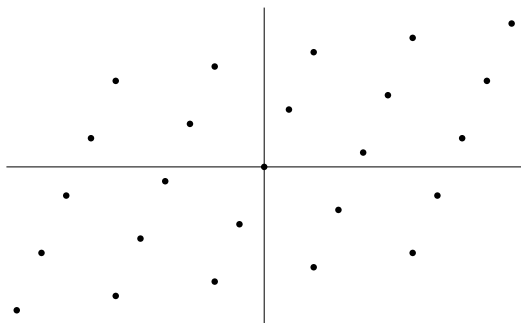
$$V(L) = \{z \in \mathbb{C} : |z| \leq |z - \omega| \text{ for all } \omega \in L\}$$

Sometimes this is also called the **Dirichlet region** or **Wigner-Seitz cell** of the lattice. It is either a rectangle or a hexagon.

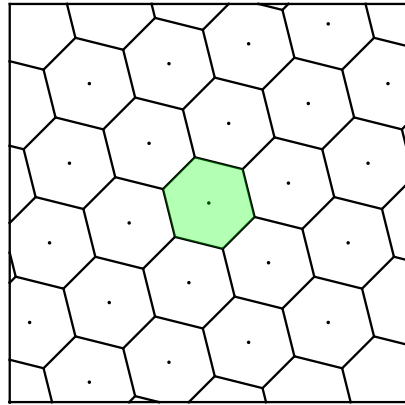
For nondegenerate $L \in \mathcal{L}$, the homeomorphism f is defined as follows. Choose a vertex v of $V(L)$. If L is rectangular, the minimum distance between v and points of L is obtained generically on two lattice points. If L is hexagonal, the minimum distance is obtained generically on three lattice points. Consider the set of two or three lines connecting v to the closest lattice points. Translating L so that v is at the origin, we obtain two or three lines passing through the origin. It is clear that these lines do not depend on the choice of vertex v and are the same for any L' homothetic to L . Since lines passing through the origin are points in $\text{RP}^1 \cong S^1$, we have associated with each nondegenerate lattice L a subset $f(L) \in \exp_3 S^1$.

Suppose instead that L is a degenerate lattice, so that L is contained within a line in RP^1 passing through the origin. We define f for degenerate lattices by sending L to this line.

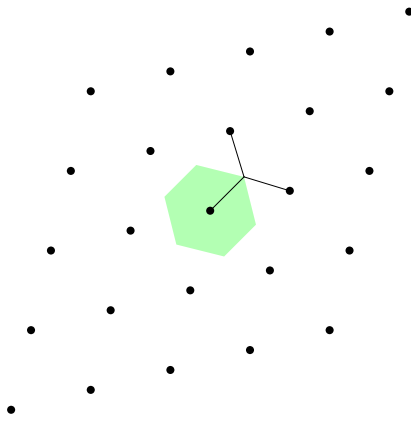
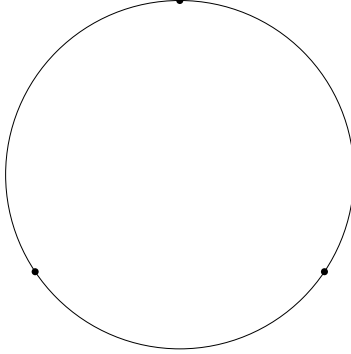
For both degenerate and nondegenerate L , the verification of the continuity of f is straightforward. Several steps of the homeomorphism for nondegenerate L are shown in Figure 3.1.



(a) A nondegenerate lattice in the plane.



(b) The Voronoi tessellation of the lattice, with a single hexagonal Voronoi cell selected.

(c) The three closest lattice points to any vertex of the cell define three lines in \mathbb{RP}^1 .(d) The three lines in $\mathbb{RP}^1 \cong S^1$ define three points on the circle.Figure 3.1: Various stages of the homeomorphism $\mathcal{L} \rightarrow \exp_3 S^1$.

3.3 Visualizing the Generators of B_3 in $\exp_{\{2,3\}} S^1$

Observe that the homeomorphism $f : \mathcal{L} = \mathcal{L}_0 \cup \mathcal{L}_1 \rightarrow \exp_3 S^1$ sends the subspace \mathcal{L}_0 to $\exp_1 S^3$ and the subspace \mathcal{L}_1 to the 2 and 3 point elements of $\exp_3 S^1$. We will denote this subspace of 2 and 3 point elements as $\exp_{\{2,3\}} S^1$.

In Chapter 2, we showed that $\pi_1(S^3 \setminus K)$ was the braid group B_3 , and that the trefoil knot K corresponded to degenerate lattices under the homeomorphism $\mathcal{L} \rightarrow S^3$. Thus we have that

$$\pi_1(\exp_{\{2,3\}} S^1) = \pi_1(\mathcal{L}_1) = \pi_1(S^3 \setminus K) = B_3$$

We now wish to describe the generators σ_1 and σ_2 of B_3 visually in $\exp_{\{2,3\}} S^1$. That

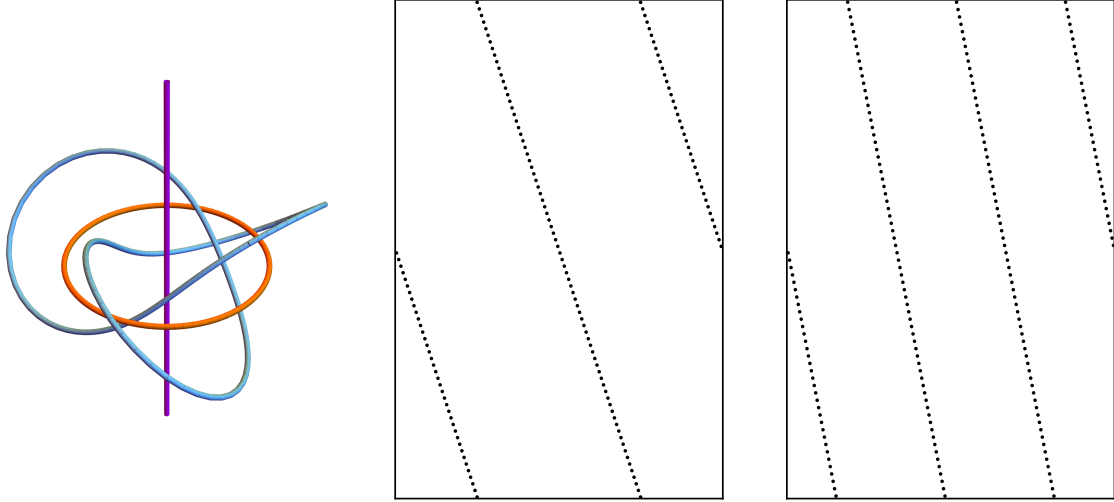


Figure 3.2: The knot complement space $S^3 \setminus K$ has a fundamental group generated by two loops x and y , shown in the left figure as the orange and pink loops, respectively (the pink strand is a loop according to the decomposition of S^3 as $S^1 \times D^2 \cup D^2 \times S^1$). The trefoil knot K is shown in blue. On the right, we visualize these generators as string cheese diagrams by pushing the generators through the sequence of homeomorphisms from S^3 to $\exp_3 S^1$, where they present as a half or third twist of equally spaced points.

is, we wish to find representatives of the path classes σ_1 and σ_2 .

In computing the fundamental group of $S^3 \setminus K$, we understood the path classes generating a group $\langle x, y : x^2 = y^3 \rangle \cong B_3$. The generator x was a path through the axis of a particular solid torus in S_3 , while y was a large loop linking the hole of the torus. Explicitly, we can parametrize these paths by $(e^{i\theta}, 0)$ and $(0, e^{i\theta})$ where $\theta \in [0, 2\pi]$. Pushing these paths via homeomorphisms $S^3 \rightarrow \mathcal{L} \rightarrow \exp_3 S^1$ yields two paths in $\exp_3 S^1$: a “half twist” and “third twist” of two or three equally spaced points, respectively.

We visualize these paths in Figure 3.2 using a style of planar diagram we call a **string cheese diagram**. In a string cheese diagram, the horizontal axis is scaled from 0 to 2π and opposite edges of the diagram are identified. Each horizontal slice of the diagram contains two or three points, and thus represents a point in $\exp_{\{2,3\}} S^1$. The vertical axis is scaled from the beginning to the end of a loop in $\exp_{\{2,3\}} S^1$, which will start and end on the same two or three points (i.e. the same single element of $\exp_{\{2,3\}} S^1$). The aesthetic of a continuous path in these diagrams is striking; we see that a path may collapse from three points to two points, or split from two points to three points à la “string cheese”.

A string cheese diagram is most useful for understanding compositions of paths that share a common basepoint, like the elements in a fundamental group. The composition of paths in $\pi_1(\exp_{\{2,3\}} S^1)$ is computed by simply stacking multiple string cheese

diagrams one after another. In this sense, the string cheese diagrams are in the same spirit as other visual calculi, such as the diagrammatic computations found of the braid group, of the Temporly-Lieb algebra, or in Paweł Sobociński’s “Graphical Linear Algebra” [Paw]. An example of path composition in $\exp_{\{2,3\}} S^1$ will be shown shortly.

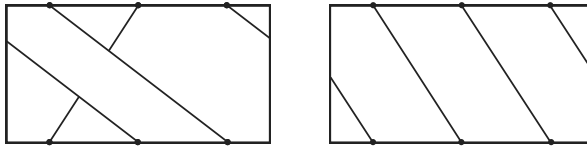


Figure 3.3: The representatives of the generators x and y of $\exp_{\{2,3\}} S^1$, modified to share a common basepoint.

To employ these diagrams in our analysis of the generators of $\pi_1(\exp_{\{2,3\}} S^1)$, we first modify the half and third twist generators from Figure 3.2 to share a common basepoint. These modified loops are shown in Figure 3.3. Then, using the inverse of the isomorphism $\pi_1(S^3 \setminus K) \rightarrow B_3$ defined in (2.1), we have that

$$\begin{aligned}\sigma_1 &= y^{-1}x \\ \sigma_2 &= x^{-1}y^2.\end{aligned}$$

The compositions $y^{-1}x$ and $x^{-1}y^2$ are shown in Figure 3.4, which yield diagrams of the braid group generators σ_1 and σ_2 that we seek. The diagrams for the inverses of σ_1 are σ_2 are shown in Figure 3.5.

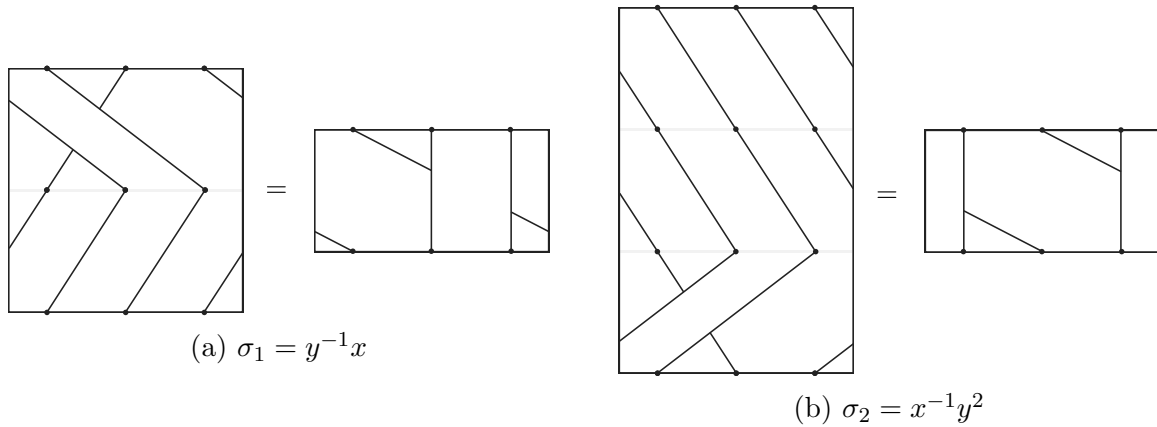
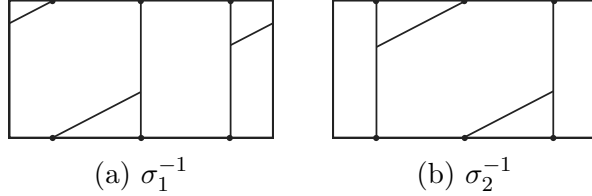
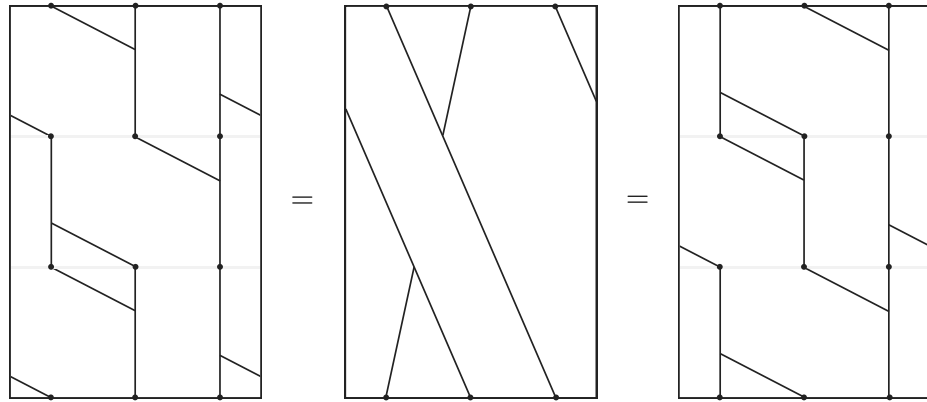


Figure 3.4: Computing the braid group generators in $\exp_{\{2,3\}}$ via composing string cheese diagrams.

The braid group B_3 has a single relation, which we saw visualized Figure 2.4. We can now visualize this same relation in $\exp_{\{2,3\}} S^1$ using via string cheese diagrams. The relation is shown in Figure 3.6.

Figure 3.5: Representatives for the inverse generators σ_1^{-1} and σ_2^{-1} of $\pi_1(\exp_{\{2,3\}} S^1)$.Figure 3.6: The braid relation $\sigma_1\sigma_2\sigma_1 = \sigma_2\sigma_1\sigma_2$ in $\pi_1(\exp_{\{2,3\}} S^1)$.

3.4 Diagrammatic Decompositions of Hyperbolic Subset Loops

Previously we saw that the periodic orbits of a dynamical system in \mathcal{L}_1 were in bijection with conjugacy classes of hyperbolic elements in $\mathrm{PSL}_2\mathbb{Z}$, and that each conjugacy class determined a modular knot in $S^3 \setminus K$. We can also examine these periodic orbits as loops in $\exp_{\{2,3\}} S^1$ via the homeomorphism $\mathcal{L} \rightarrow \exp_3 S^1$. Several such loops are shown in Figure 3.7; it may be interesting to compare them to the knots in $S^3 \setminus K$ produced by the same hyperbolic matrices in Figure 2.5. When viewed in $\exp_{\{2,3\}} S^1$, we call these periodic orbits **hyperbolic subset loops**.

The path class of each of these hyperbolic subset loops is an element of the group $\pi_1(\exp_{\{2,3\}} S^1)$, which is isomorphic to the braid group B_3 . In particular, each loop is a braid word in σ_1 and σ_2 , the generators of B_3 . In the previous section, we found visual representatives for σ_1 and σ_2 . Given a diagram of a hyperbolic subset loop, can we decompose it into a word in σ_1 and σ_2 ?

We demonstrate that such a decomposition is possible with the following steps:

1. If necessary, first shift the hyperbolic subset loop diagram so that the top and bottom edges correspond to a 3-pointed element of $\exp_{\{2,3\}} S^1$. Since the diagram represents a loop, we are free to choose which point in the loop is the starting and ending point.

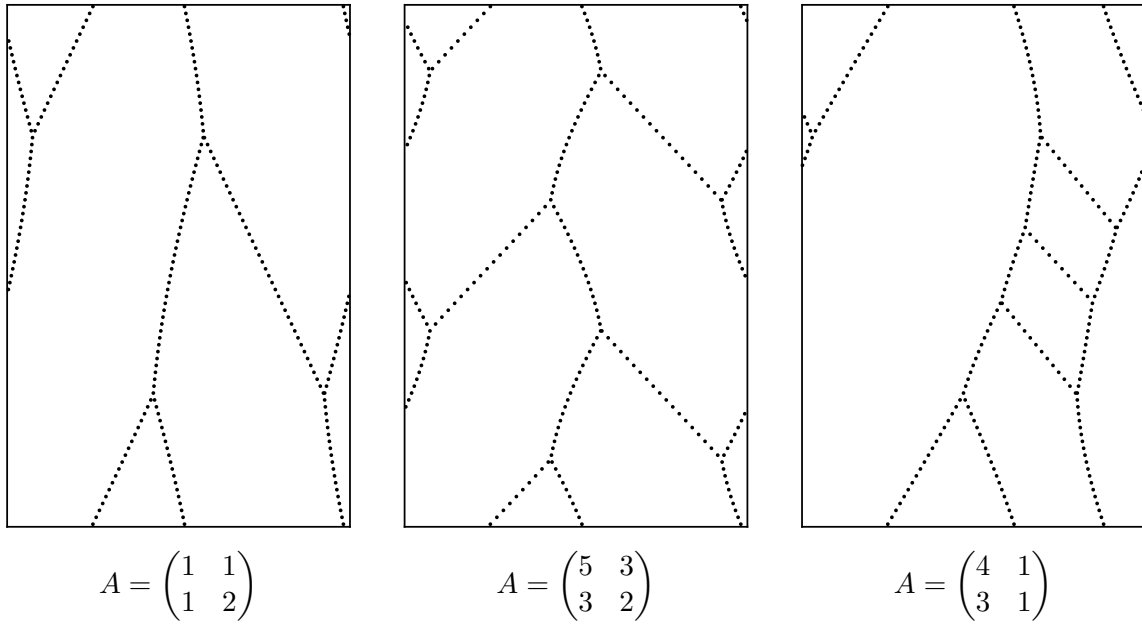


Figure 3.7: Conjugacy classes of hyperbolic $A \in \mathrm{PSL}_2\mathbb{Z}$ are in bijection with period orbits of a dynamical system in \mathcal{L} . These periodic orbits can be examined as loops in $\exp_{\{2,3\}} S^1 \approx \mathcal{L}_1$. Here, several loops are shown in $\exp_{\{2,3\}} S^1$ for various values of $A \in \mathrm{PSL}_2\mathbb{Z}$.

2. Perform a series of homotopy-class preserving deformations to simplify the diagram. These deformations must be homotopies. In particular, at no time can the deformed loop diagram have a 1-point element.
3. Identify a sequence of σ_1 and σ_2 diagrams that can be homotopy-transformed back to the diagram in the previous step.

This process is shown for two separate hyperbolic subset loop diagrams in Figure 3.8 and Figure 3.9. The results for decomposing several more diagrams are presented in Figure 3.10.

We know that every modular trefoil knot has a corresponding representation as an element of the braid group because we computed $\pi_1(S^3 \setminus K)$ directly. However, this computation was achieved via the sprawling and opaque machinery of the Seifert Van-Kampen theorem, and provides little insight into how we ought to intuit modular trefoil knots as braids. Decomposing string cheese diagrams provides us with our concrete examples of braids and their corresponding modular trefoil links. What can we now say about modular trefoil links as braids?

The braid word β_A for a modular trefoil link k_A mimics the PQ decomposition of A closely. For example, $A = PQQ$ is $\sigma_2\sigma_2\sigma_1^{-1}$ as a braid, while $A = PQQQ$ is $\sigma_2\sigma_2\sigma_2\sigma_1^{-1}$. Notice that every character in the PQ word has exactly one matching character in the braid word. These matchings vary throughout the different example braids—

sometimes Q corresponds to σ_1 in a braid word, but other times it corresponds to σ_2 —but for each individual (k_A, β_A) pairing there is some one-to-one correspondence between characters P and Q in A and characters $\sigma_i^{\pm 1}$ in β_A .

There may still exist a map between $\mathrm{PSL}_2\mathbb{Z}$ and B_3 that utilizes PQ decompositions of elements in $\mathrm{PSL}_2\mathbb{Z}$. Every braid β_A for a modular trefoil link k_A was obtained via a decomposition of the string cheese diagram for k_A . Did we make subtle and arbitrary choices in the decomposition process that affects whether P maps to σ_2^{-1} or σ_1^{-1} , and whether Q maps to σ_1 or σ_2 ? Or does the sign of the braid group generators reflect the orientation of the modular trefoil link? Or yet still, are some of these braid words equivalent? These questions remain open.

3.5 The Linking Number of Finite Subset Loops

Pushing modular knots into $\exp_{\{2,3\}} S^1$ enables the decomposition of their path classes as braid words. More generally, it also provides a rich variety of modular knots examples that can be studied in a new setting. Can we recover any of the known results about modular knots from the perspective of $\exp_{2,3} S^1$? We conclude this thesis with a conjecture concerning the linking number of hyperbolic subset loops.

Every point along a hyperbolic subset loop is a two- or three-pointed subset of S^1 . In a string cheese diagram, the two-pointed subsets of the loop are easily identified and appear only a finite number of times. At each of these two-pointed subsets, an incoming fork and outgoing fork are visible. Furthermore, the incoming strand to the outgoing fork has an orientation; it is either approaching from the left or right side of the diagram (see Figure 3.11). If the incoming strand to the outgoing fork approaches from the left in a string cheese diagram, we call the outgoing fork a **left fork**. Otherwise, the outgoing fork is a **right fork**.

Conjecture 3.2. Let m and n be the number of left and right forks, respectively, in a string cheese diagram of a modular knot k_A . Then the linking number of k_A is $m - n$.

This conjecture is motivated empirically by a large set of string cheese diagrams for which the statement holds true. Recall that every conjugacy class of a hyperbolic element of $\mathrm{PSL}_2\mathbb{Z}$ has a PQ -decomposition (Corollary 2.10), and that the trace of a matrix in $\mathrm{PSL}_2\mathbb{Z}$ is an invariant of its conjugacy class (Lemma 2.8). It's readily verified that multiplication by P or Q increases the trace of a hyperbolic PQ word. Thus to enumerate the conjugacy classes of hyperbolic elements of $\mathrm{PSL}_2\mathbb{Z}$, we can enumerate words in P and Q (taking care to omit words containing cycles and starting with PQ). In Appendix A.3, we supply a computer program that outputs a string cheese diagram given a PQ word. We produced 32 string cheese diagrams for PQ words corresponding to 32 unique conjugacy classes of elements in $\mathrm{PSL}_2\mathbb{Z}$ and verified the conjecture in each case by applying Theorem 2.16 to the PQ words and by visually inspecting the diagrams. We provide these diagrams in Appendix B.

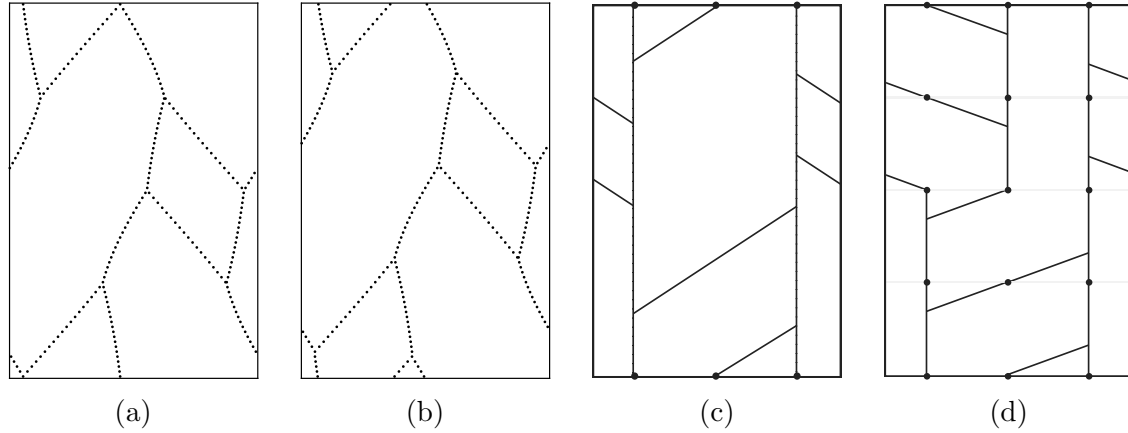


Figure 3.8: Decomposing the hyperbolic subset loop diagram for $A = \begin{pmatrix} 5 & 2 \\ 2 & 1 \end{pmatrix}$ into braid group generators. The diagram in (a) depicts the unmodified periodic orbit in \mathcal{L} corresponding to A after it has been pushed $\mathcal{L} \rightarrow \exp_{\{2,3\}} S^1$ via a homeomorphism. In (b), the diagram has been shifted so that it begins and ends on a 3-point element of $\exp_{\{2,3\}} S^1$. In (c), the diagram has been continuously deformed to represent a path within the same homotopy class. In (d), the deformed diagram has been decomposed into a sequence of σ_1 and σ_2 diagrams, whose composition is still within the same homotopy class. The sequence is the braid $\sigma_2^{-1}\sigma_2^{-1}\sigma_1\sigma_1$.

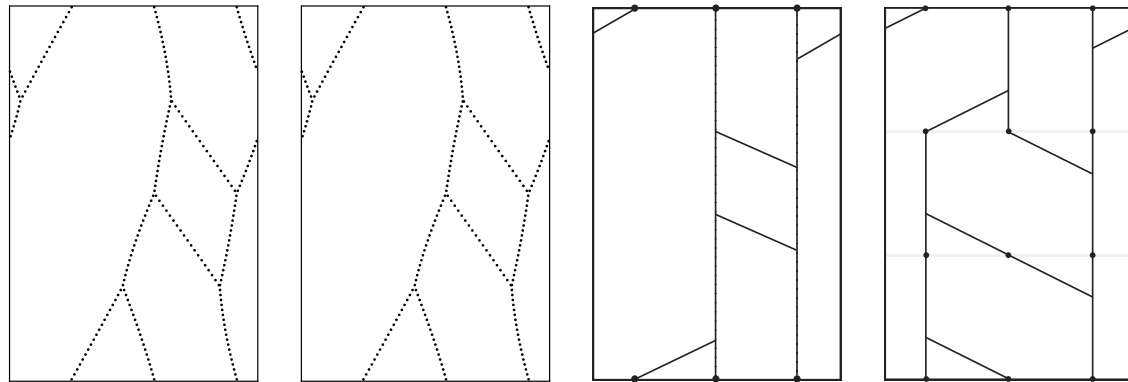


Figure 3.9: Decomposing the hyperbolic subset loop diagram for $A = \begin{pmatrix} 3 & 1 \\ 2 & 1 \end{pmatrix}$ into braid group generators, with the same process described in Figure 3.8.

hyperbolic matrix	hyperbolic subset loop decomposition
$PQ = \begin{pmatrix} 2 & 1 \\ 1 & 1 \end{pmatrix}$	$\sigma_2\sigma_1^{-1}$
$PQQ = \begin{pmatrix} 3 & 1 \\ 2 & 1 \end{pmatrix}$	$\sigma_2\sigma_2\sigma_1^{-1}$
$PQQQ = \begin{pmatrix} 4 & 1 \\ 3 & 1 \end{pmatrix}$	$\sigma_2\sigma_2\sigma_2\sigma_1^{-1}$
$PQQQQ = \begin{pmatrix} 5 & 1 \\ 4 & 1 \end{pmatrix}$	$\sigma_2\sigma_2\sigma_2\sigma_2\sigma_1^{-1}$
$PPPQ = \begin{pmatrix} 4 & 3 \\ 1 & 1 \end{pmatrix}$	$\sigma_2^{-1}\sigma_1\sigma_2^{-1}\sigma_2^{-1}$
$PPPQQ = \begin{pmatrix} 7 & 3 \\ 2 & 1 \end{pmatrix}$	$\sigma_2^{-1}\sigma_2^{-1}\sigma_1\sigma_1\sigma_2^{-1}$
$PPPPQ = \begin{pmatrix} 5 & 4 \\ 1 & 1 \end{pmatrix}$	$\sigma_2^{-1}\sigma_2^{-1}\sigma_2^{-1}\sigma_1\sigma_2^{-1}$
$PPQ = \begin{pmatrix} 3 & 2 \\ 1 & 1 \end{pmatrix}$	$\sigma_1\sigma_2^{-1}\sigma_2^{-1}$
$PPQQ = \begin{pmatrix} 5 & 2 \\ 2 & 1 \end{pmatrix}$	$\sigma_2^{-1}\sigma_2^{-1}\sigma_1\sigma_1$
$PPQQQ = \begin{pmatrix} 7 & 2 \\ 3 & 1 \end{pmatrix}$	$\sigma_2^{-1}\sigma_2^{-1}\sigma_1\sigma_1\sigma_1$
$PQPQ = \begin{pmatrix} 5 & 3 \\ 3 & 2 \end{pmatrix}$	$\sigma_2\sigma_1^{-1}\sigma_2\sigma_1^{-1}$
$PQPQP = \begin{pmatrix} 5 & 8 \\ 3 & 5 \end{pmatrix}$	$\sigma_2^{-1}\sigma_2^{-1}\sigma_1\sigma_2^{-1}\sigma_1$

Figure 3.10: Decompositions of hyperbolic subset loops corresponding to twelve hyperbolic matrices. Each matrix is in a unique conjugacy class, and thus produces a unique hyperbolic subset loop.

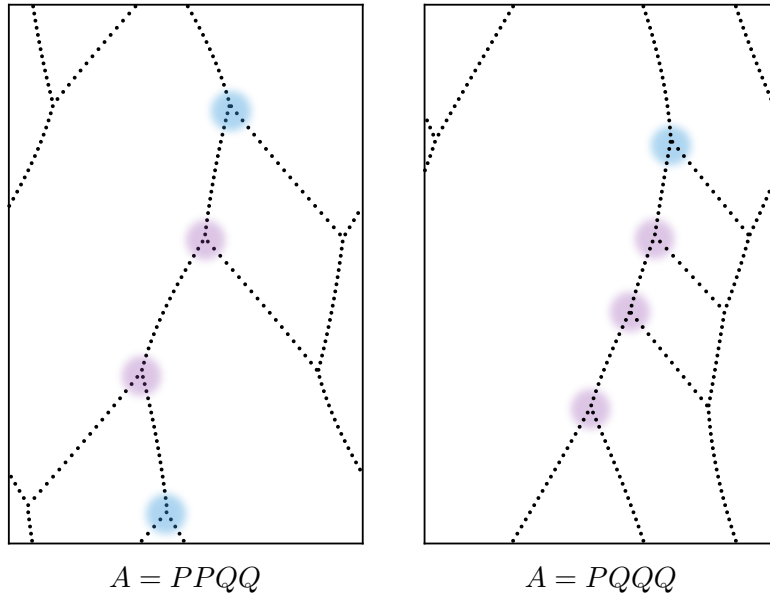


Figure 3.11: Two string cheese diagrams corresponding to the modular knot k_A where $A \in \mathrm{PSL}_2\mathbb{Z}$. The outgoing forks in each diagram are highlighted. If the incoming strand to an outgoing fork approaches from the left, we call the fork a **left fork** (highlighted in blue). Otherwise, it is a **right fork** (highlighted in purple). We conjecture that the linking number of a modular knot k_A is the number of left forks minus the number of right forks in a string cheese diagram for k_A .

Appendix A

Computational Exploration of Homeomorphisms

Steve Jobs believed that a computer is a “bicycle for the mind” [KL90]. We can’t tell computers what to think, but we can employ them to make our own thinking more efficient. This observation is now so widely realized as to be banal—in every other field besides mathematics, at least. Mathematics, however, remains less affected by developments in computing.

By its nature, math seeks knowledge about objects that defy computational interpretation. It seeks to describe properties of all real numbers and not just those that we can store in a finite bank of computer memory. While some progress has been made in articulating mathematical knowledge as computer programs, computers will continue to be of secondary importance in mathematics for the foreseeable future. We can, however, use computers to generate intuition and to suggest what purely analytical questions we might ask next.

The results in this document were explored and understood via computer programming. What follows now is a “literate programming” description of the relevant Mathematica programs [Knu94]. Some knowledge of Mathematica programming is assumed. These programs and other digital supplements to this thesis will be made available on the Reed Electronic Thesis Archive¹ as well as on GitHub².

¹<https://rdc.reed.edu/c/etheses/home/>

²<https://github.com/chnn>

A.1 Visualizing a Dynamical System in the Space of Lattices

A lattice is uniquely defined by its generators, a pair of complex numbers. This suggests we can encode lattices programmatically in a simple manner as $\{w_1, w_2\}$, where w_1 and w_2 are the complex generators.

In Section 1.1, we considered a lattice produced by a 2×2 matrix acting point-wise upon the standard square lattice, $\mathbb{Z} \oplus \mathbb{Z}$. Given a lattice, we can find this corresponding matrix:

```
latticeToMtx[m_] := m // ReIm // Transpose;
```

We can also convert back to a lattice from the matrix form:

```
mtxToLattice[m_] := (Complex @@ #)& /@ Transpose[m];
```

These are just simple accessors to get data representing a lattice into a convenient shape. We can now describe the dynamical system of Proposition 1.1. Suppose that $A \in PSL_2\mathbb{Z}$, and let P such that $PAP^{-1} = \delta_t$, where δ_t is defined as in (1.1). Then P is a matrix whose columns are the eigenvectors of A , thus we can compute the lattice corresponding to P with the function

```
latticeForModularMtx[a_] := a // Eigenvectors // N // Transpose // Inverse
                           // mtxToLattice;
```

where a is the Mathematica representation of A . Remember that we obtain the dynamical system of interest by acting upon P via δ_t for continuously increasing t .

To observe a periodic orbit in this system, we need a programmatic method for obtaining the orbit time. That is, we wish to find a minimal $T > 0$ such that $\delta_T P = P$. We know that $PAP^{-1} = \delta_T$ is a diagonal matrix with diagonal entries being eigenvalues of A . And since

$$\delta_T = \begin{pmatrix} \exp(T) & 0 \\ 0 & \exp(-T) \end{pmatrix}$$

these eigenvalues are in fact $\exp(T)$ and $\exp(-T)$. Thus we can take the logarithm of the absolute value of either eigenvalue to obtain the orbit time T . In Mathematica, we do so with the following function:

```
orbitTimeForModularMtx[m_] := m // Eigenvalues // N // First // Abs // Log;
```

With the appropriate matrix P corresponding to some $A \in \mathrm{PSL}_2\mathbb{Z}$ and the orbit time readily available, we can now encode the path of a periodic orbit in the space of lattices. First, we define a quick utility function for δ_t :

```
deltaT[t_] := {{E^t, 0}, {0, E^-t}} // N;
```

Then an ordered list of points along the periodic orbit can be computed as follows:

```
assocLatticeLoop[mtx_, res_: 100] := Module[{p, t},
  p = latticeToMtx[latticeForModularMtx[mtx]];
  t = orbitTimeForModularMtx[mtx];
  Table[mtxToLattice[deltaT[u].p], {u, 0, t, t / res}]
];
```

There are, of course, infinitely many points along the path of the periodic orbit, of which we can only compute a finite number. We parameterize the amount of points along the path to compute with the resolution parameter `res`.

How can we visualize these periodic orbits? Each point in the periodic orbit is a lattice, and we can readily visualize a subset of each lattice in the plane. Thus a natural visualization choice for the periodic orbits is an animation, with each frame being a depiction of a lattice in the plane. The following function produces a subset of the points in a lattice:

```
latticePoints[{w1_, w2_}, size_: 1] := ReIm /@ Flatten[Table[m w1 + n w2,
  {m, Range[-size, size]}, {n, Range[-size, size]}]];
```

Then the desired animation is produced by:

```
visualizeLatticeLoop[ls_] := ListAnimate[ListPlot[latticePoints[#, 100],
  PlotRange -> {{-2, 2}, {-2, 2}}]& /@ assocLatticeLoop[ls]]
```

It's difficult to print a movie onto a piece of paper, so we show a static adaptation of this animation in Figure 1.2.

A.2 Coding the Homeomorphism from $\mathcal{L} \rightarrow S^3$

We now have a program capable of realizing the periodic orbits of a dynamical system in the space of lattices. In the homeomorphic space S^3 , these periodic orbits appear

as links with the trefoil. In this section, we will code the homeomorphism from \mathcal{L} to S^3 described in Section 2.2, and use it to visualize links with the trefoil.

The homeomorphism $\mathcal{L} \rightarrow S^3$ sends a lattice L to a rescaled version of the complex tuple $(G_4(L), G_6(L))$, where

$$G_k(L) = \sum_{\omega \in L, \omega \neq 0} \omega^{-k}$$

A nontrivial lattice L contains infinitely many points ω , presenting a potential challenge in computing $G_k(L)$. The series for $G_4(L)$ and $G_6(L)$ do converge however, and for nondegenerate lattices we can compute the tuple $(G_4(L), G_6(L))$ using Mathematica's `WeierstrassInvariants` function. The `WeierstrassInvariants` function (more commonly used in cryptographic applications) returns two special constants g_2 and g_3 associated with a lattice. These are related to $G_4(L)$ and $G_6(L)$ by $g_2(L) = G_4(L)/60$ and $g_3(L) = G_6(L)/140$. Thus the Mathematica function

```
nondegenGTuple[{w1_, w2_}] := N[WeierstrassInvariants[{w1/2, w2/2}] *  
  → {1/60, 1/140} // Chop;
```

returns our desired point $(G_4(L), G_6(L))$ for nondegenerate $L \in \mathcal{L}$. What about degenerate lattices? In this case, the series $G_k(L)$ converge fast enough that we can leverage a straightforward numerical approach. We start computing the infinite series from the origin outwards, and let Mathematica determine when we have reached reasonable numeric accuracy:

```
degenEisensteinSeries[c_, k_] := N[Sum[(n c)^{-k} + (-n c)^{-k}, {n,  
  → ∞[Infinity]}]];  
  
degenGTuple[c_] := {degenEisensteinSeries[c, 4], degenEisensteinSeries[c,  
  → 6]};
```

Now, the next step in the homeomorphism is to rescale the tuple $(G_4(L), G_6(L))$ so that it lies in $S^3 = \{(u, v) \in \mathbb{C} : |u|^2 + |v|^2 = 1\}$. Recall that for any real number $t > 0$ and lattice L , we have that

$$G_4(tL) = t^{-4}G_4(L)$$

and

$$G_6(tL) = t^{-6}G_6(L)$$

Thus we solve for the appropriate scaling factor t so that $(G_4(tL), G_6(tL))$ is in S^3 :

```
gTupleScaleFactor[{g4_, g6_}] := t /. Solve[Norm[t^{-4} g4]^2 + Norm[t^{-6}  
  → g6]^2 == 1 && t ∈ Reals && t > 0, t][[1]] // Quiet;
```

We're almost ready to code the complete homeomorphism $\mathcal{L} \rightarrow S^3$. The last gadget we need is a utility function to check if a lattice is degenerate, so that we know when to branch into our separate `nondegenGTuple` and `degenGTuple` functions. A degenerate lattice either has a zero generator, or has rank one in matrix form.

```
isDegen[{w1_, w2_}] := w1 == 0 || w2 == 0 || MatrixRank[{ReIm[w1],
→ ReIm[w2]}] == 1;
```

Now we can wire up our previously defined functions to form the complete homeomorphism.

```
latticeToS3[l_] := Module[{gTuple, t},
  gTuple = If[isDegen[l], degenGTuple[degenGenerator[l]],
  → nondegenGTuple[l]];
  t = gTupleScaleFactor[gTuple];
  {t^-4, t^-6} * gTuple
];
```

As discussed in Section 2.2, all degenerate lattices in \mathcal{L} present as a trefoil when viewed in S^3 . We can see this via our coded homeomorphism as follows. First, we define a function that will help us parameterize a path through all degenerate lattices.

```
degenLatticeForAngle[rad_] := N[{Complex @@ radToR2[rad], Complex @@
→ radToR2[rad]}];
```

Since S^3 lies within four-dimensional space, we also need to stereographically project points of S^3 into \mathbb{R}^3 before we can visualize them.

```
projS3ToR3[{z1_, z2_}] := {Re[z1]/(1 - Im[z2]), Im[z1]/(1 - Im[z2]),
→ Re[z2]/(1 - Im[z2])};
```

Now we can generate the points of the trefoil knot:

```
trefoilPoints = Table[degenLatticeForAngle[r] // latticeToS3 //
→ projS3ToR3, {r, 0, Pi, 0.02}];
```

And then visualize the trefoil, as shown in Figure 2.1:

```
trefoilPlot = Graphics3D[{Thick, Blue, Tube[trefoilPoints]}, Boxed ->
→ False]
```

What of the trefoil links produced by periodic orbits of the dynamical system in \mathcal{L} ? We can view them alongside the trefoil with the following function, which generates the periodic orbit in \mathcal{L} corresponding to some hyperbolic mtx , pushes it through the homeomorphism to S^3 , then visualizes it alongside the `trefoilPlot` via stereographic projection.

```
plotAssocKnot[mtx_ , res_]:= Show[Graphics3D[{Thick, ,
  Tube[projS3ToR3 /@ latticeToS3 /@ assocLatticeLoop[mtx, res] }], ,
  trefoilPlot];
```

This function produces the visualizations in Figure 2.5.

A.3 Coding the Homeomorphism from $\mathcal{L} \rightarrow \exp_3 S^1$

The homeomorphism from \mathcal{L} to $\exp_3 S^1$ described in Section 3.2 is already algorithmic in nature. Briefly, we recall the steps of the homeomorphism for a nondegenerate lattice L :

1. Select a single cell in the Voronoi partition of L
2. Select any vertex of that cell, and translate the entire lattice so that this vertex is at the origin
3. Consider the two or three lines connecting the vertex to the next closest points in the lattice
4. These lines define two or three points in RP^1 , which is homeomorphic to S^1

We quite literally translate this process into a Mathematica procedure as follows:

```
nondegenToExpS1[{w1_ , w2_}] := Module[{points, d, cell, vertex, sorted,
  isRectangular, minPoints, lines},
  points = latticePoints[{w1, w2}, latticeSize];
  cell = SelectFirst[MeshPrimitives[VoronoiMesh[points], 2], ({0,0}
  [[Element] #]]];
  vertex = cell[[1,1]];
  sorted = Sort[points, (EuclideanDistance[vertex, #1] <
    EuclideanDistance[vertex, #2])&];
  isRectangular = Length[DeleteDuplicates[cell[[1]]]] == 4;
  minPoints = Take[sorted, If[isRectangular, 2, 3]];
  lines = Map[(Line[{vertex, #}])&, minPoints];
  Map[({#[[1,2]] - #[[1,1]] // r2ToRad // radOnHalfCircle //
  halfToFullCircle})&, lines]
];
```

Here we have used a few utility functions which define the homeomorphism between RP^1 and S^1 . The function `r2ToRad` gives the angle between a vector in \mathbb{R}^2 and the positive x -axis:

```
r2ToRad[p_] := Complex @@ p // Arg;
```

The functions `radOnHalfCircle` and `halfToFullCircle` are then used to translate this angle appropriately to S^1 :

```
radOnHalfCircle[rad_] := If[rad >= Pi, Pi - rad, rad];
halfToFullCircle[rad_] := Rescale[rad, {0, Pi}, {0, 2 Pi}];
```

For the degenerate lattice case, the homeomorphism $\mathcal{L} \rightarrow \exp_3 S^1$ is more straightforward. A degenerate lattice defines a line through the origin via either of its generators c . We take the line in RP^1 and translate it to $\exp_3 S^1$ as before.

```
degenToExpS1[c_] := {Arg[c] // radOnHalfCircle // halfToFullCircle};
```

Now we can simply connect the degenerate and nondegenerate cases as before by branching on the `isDegen` function:

```
latticeToExpS1[lattice_] := If[isDegen[lattice],
→ degenToExpS1[degenGenerator[lattice]], nondegenToExpS1[lattice]]
```

With the homeomorphism $\mathcal{L} \rightarrow \exp_3 S^1$ in hand, we also need a method for visualizing paths in $\exp_3 S^1$. The following code is rather terse, but the idea is simple. We associate each point in the path (a subset of S^1 , i.e. a subset of numbers between 0 and 2π) with an increasing value r using `zipWithIncreasing`. Then we map over each zipped ($x \in \exp_{\{2,3\}} S^1, r \in [0, 1]$) tuple to produce several $(x_i \in S^1, r)$ tuples. We flatten the result to remove one superfluous level of nesting. Finally, we plot the points in the plane, with the y direction of the plot corresponding to the increasing r values and the x direction corresponding to the position of the subset points on the circle.

```
zipWithIncreasing[xs_, r0_ : 0, r1_ : 1] := Map[(xs[[#]], N[r0 + (# (r1 -
→ r0))/Length[xs]]) &, Range[Length[xs]]];
flatViz[xs_] := Module[{zipped, split, points},
(* Map points {a, b, c} to {{a, b, c}, r} with r increasing *)
zipped = zipWithIncreasing[xs, 1, 0];
```

```
(* Map points {{a, b, c}, r} to {{a, r}, {b, r}, {c, r}} *)
split = Function[p, Map[({Mod[#, 2 Pi], p[[2]]})&, p[[1]]]];

(* Flatten a the resulting list of lists by one level *)
points = Flatten[Map[split, zipped], 1];

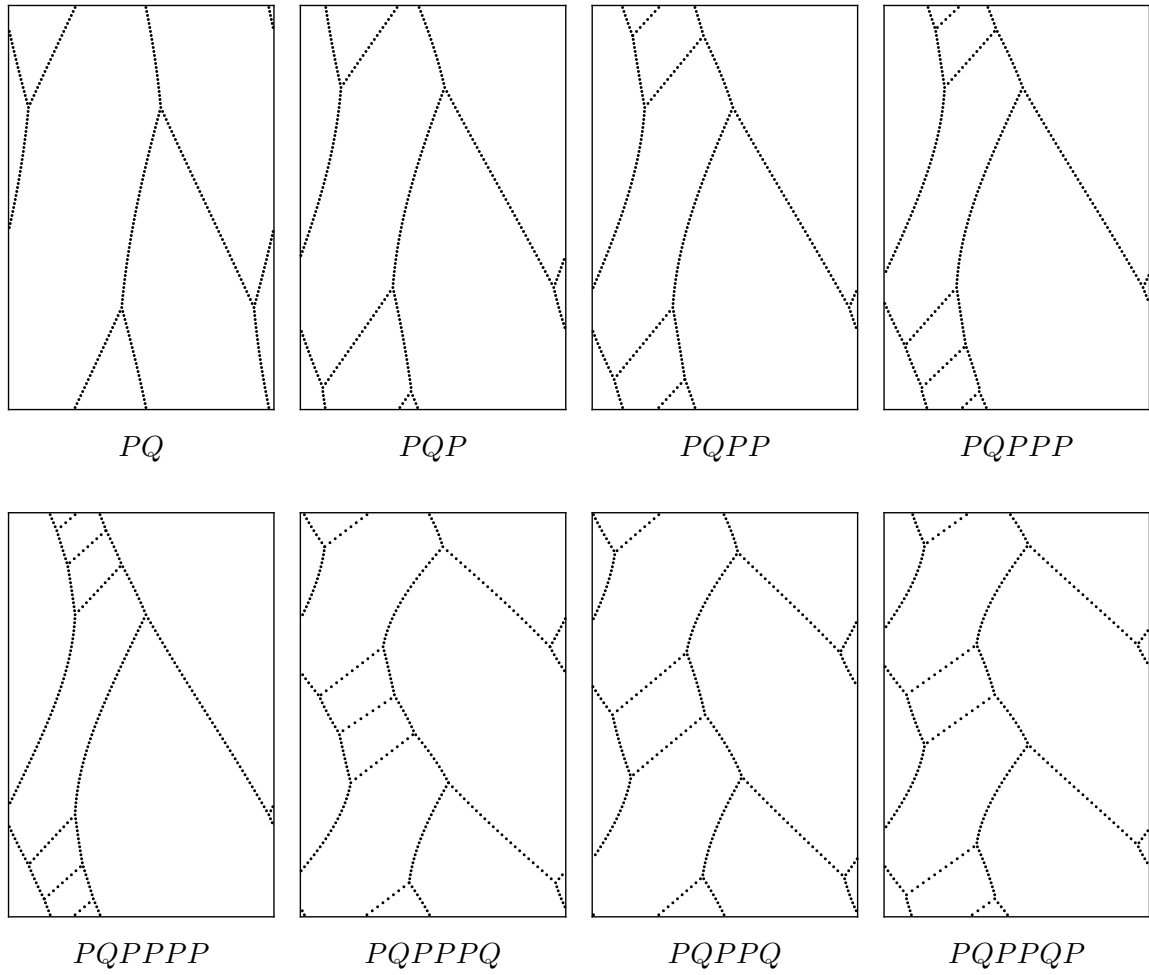
(* Display the processed points *)
Graphics[{Thickness[0.005],
    Line[{{0, 0}, {2 Pi, 0}}],
    Line[{{0, 0}, {0, 1}}],
    Line[{{2 Pi, 0}, {2 Pi, 1}}],
    Line[{{0, 1}, {2 Pi, 1}}],
    Point[points]}, AspectRatio -> 3/2]
];
```

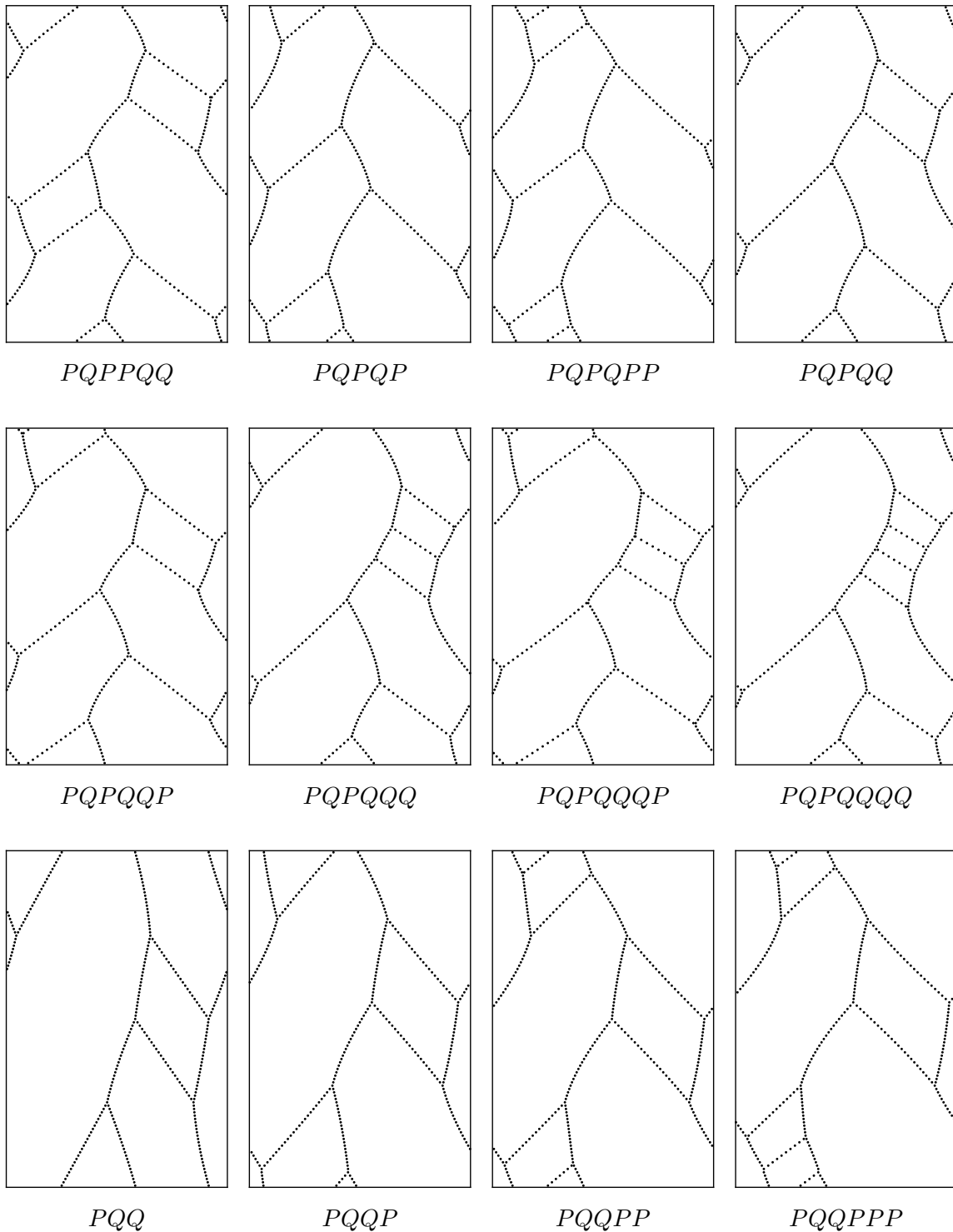
This method produces the subset loop visualizations shown in Figure 3.7.

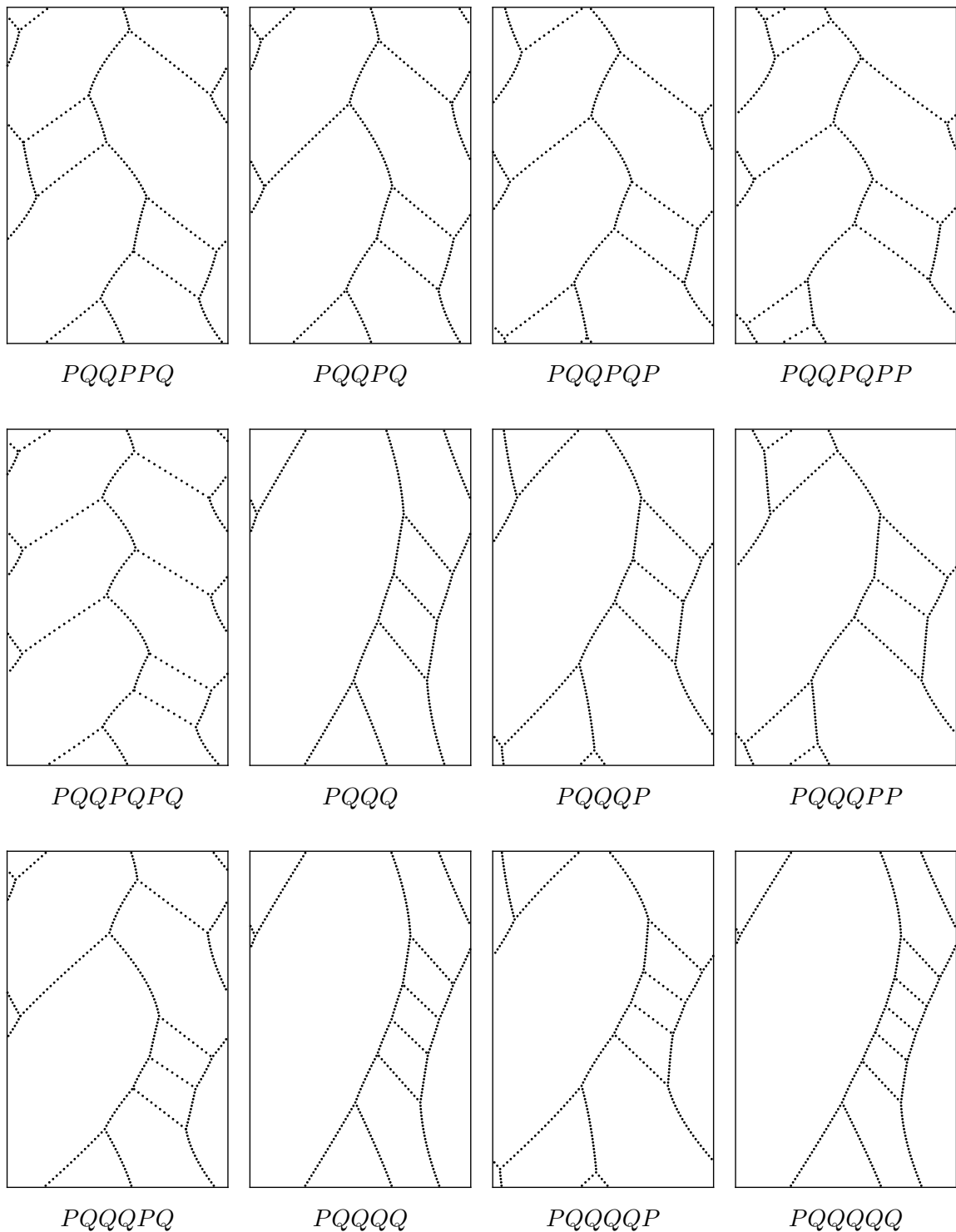
Appendix B

Supplemental Data

The following 32 string cheese diagrams are provided in support of Conjecture 3.2.







Bibliography

- [Arn66] V. Arnold. “Sur la géométrie différentielle des groupes de Lie de dimension infinie et ses applications à l’hydrodynamique des fluides parfaits”. In: *Ann. Inst. Fourier (Grenoble)* 16.fasc. 1 (1966), pp. 319–361. ISSN: 0373-0956. URL: http://www.numdam.org/item?id=AIF_1966__16_1_319_0.
- [AS64] M. Abramowitz and I.A. Stegun. *Handbook of Mathematical Functions: With Formulas, Graphs, and Mathematical Tables*. Applied mathematics series. Dover Publications, 1964. ISBN: 9780486612720.
- [BW14] Bruce Bartlett and Simon Willerton. *The Modular Flow on the Space of Lattices*. Apr. 7, 2014. URL: https://golem.ph.utexas.edu/category/2014/04/the_modular_flow_on_the_space.html (visited on 04/20/2018).
- [Ghy07] Étienne Ghys. “Knots and dynamics”. In: *International Congress of Mathematicians. Vol. I*. Eur. Math. Soc., Zürich, 2007, pp. 247–277. URL: <https://doi.org/10.4171/022-1/11>.
- [Hat02] Allen Hatcher. *Algebraic topology*. Cambridge University Press, Cambridge, 2002, pp. xii+544. ISBN: 0-521-79160-X; 0-521-79540-0.
- [Kat92] S. Katok. *Fuchsian Groups*. Chicago Lectures in Mathematics. University of Chicago Press, 1992. ISBN: 9780226425825. URL: <https://books.google.com/books?id=pJ2Se3tCr-cC>.
- [KL90] Julian Krainin and Michael R. Lawrence. *Memory & Imagination: New Pathways to the Library of Congress*. 1990.
- [Knu94] Donald E. Knuth. *Literate Programming*. Stanford, California: CSLI, 1994.
- [LG] Jos Leys and Étienne Ghys. *Lorenz and modular flows: a visual introduction. A tangled tale linking lattices, knots, templates, and strange attractors*. URL: http://www.josleys.com/articles/ams_article/Lorenz3.htm (visited on 11/06/2017).
- [Mil68] J.W. Milnor. *Singular Points of Complex Hypersurfaces*. Annals of mathematics studies. Princeton University Press, 1968. ISBN: 9780691080659. URL: <https://books.google.com/books?id=cuAAFbBYlSsc>.
- [Mos04] Jacob Mostovoy. “Lattices in \mathbb{C} and Finite Subsets of a Circle”. In: *The American Mathematical Monthly* 111.4 (Aug. 2004), pp. 357–360.

-
- [Paw] Fabio Zanasi Paweł Sobociński Filippo Bonchi. *Graphical Linear Algebra*. URL: <https://graphicallinearalgebra.net/> (visited on 03/23/2018).
 - [Rad56] Hans Rademacher. “Zer Theorie der Dedekindschen Summen”. In: *Mathematische Zeitschrift* 63 (1956), pp. 445–463.
 - [Ran77] Robert A Rankin. *Modular forms and functions*. Cambridge University Press, 1977.
 - [RG72] Hans Rademacher and Emil Grosswald. *Dedekind Sums*. Carus Mathematical Monographs. Washington: Mathematical Association of America, 1972.
 - [Ser73] Jean-Pierre Serre. *A Course in Arithmetic*. Vol. 7. Graduate Texts in Mathematics. Springer, New York, 1973. ISBN: 978-0-387-90040-7.
 - [Sil94] J.H. Silverman. *Advanced Topics in the Arithmetic of Elliptic Curves*. Graduate texts in mathematics. Springer-Verlag, 1994. ISBN: 9780387943251. URL: <https://books.google.com/books?id=dnZ0Vdo-7BsC>.
 - [Sti93] John Stillwell. *Classical topology and combinatorial group theory*. Second. Vol. 72. Graduate Texts in Mathematics. Springer-Verlag, New York, 1993, pp. xii+334. ISBN: 0-387-97970-0. URL: <https://doi.org/10.1007/978-1-4612-4372-4>.
 - [Tao10] Terence Tao. *The Euler-Arnold equation*. June 7, 2010. URL: <https://terrytao.wordpress.com/2010/06/07/the-euler-arnold-equation> (visited on 04/17/2018).